SEMMELWEIS EGYETEM
DOKTORI ISKOLA

Ph.D. értekezések

3145.

KOVÁCS KINGA BERNADETT

Celluláris és molekuláris élettan

című program

Programvezető: Dr. Hunyady László, egyetemi tanár

Témavezető: Dr. Balla András, egyetemi docens

Angiotensin II Upregulates the Expression of an Oxysterol Producing Enzyme: Cholesterol-25-Hydroxylase in Vascular Smooth Muscle Cells

PhD thesis

Kinga Bernadett Kovács

Semmelweis University Doctoral School

Division of Molecular Medicine

Supervisor: András Balla, PhD

Official reviewers: Róza Zákány, PhD

Szabolcs Sipeki, PhD

Head of the Complex Examination Committee:

Szabolcs Várbíró, MD, PhD, Med., Habil.

Members of the Complex Examination Committee:

Éva Ruisanchez, MD, PhD

Anita Alexa, PhD

Budapest

2024

Table of contents

List of Abbreviations

25-HC	25-hydroxycholesterol
27-HC	27-hydroxycholesterol
7-K	7-ketocholesterol
7α-HC	7α-hydroxycholesterol
7α,25-OHC	7α,25-Dihydroxycholesterol
α-epoxide	cholesterol-5α,6α-epoxide
ABC	ATP-binding cassette transporter
ACE	angiotensin converting enzyme
ADAM17	a disintegrin and metalloprotease 17
AngI	angiotensin I
AngII	angiotensin II
APS	ammonium persulfate
AT1R	type-1 angiotensin II receptor
ATF2	activating transcription factor-2
cAMP	cyclic adenosine monophosphate
cDNA	complementary deoxyribonucleic acid
CH25H	cholesterol-25-hydroxylase
CPI-17	protein phosphatase 1 regulatory subunit 14
CVD	cardiovascular disease
DAG	diacylglycerol
DMSO	dimethyl sulfoxide
DNA	deoxyribonucleic acid
dNTP	deoxynucleotide triphosphate
DPI	diphenyleneiodonium chloride
DUSP	dual-specificity MAPK phosphatase
DUSP10	dual-specificity MAPK phosphatase 10
DUSP5	dual-specificity MAPK phosphatase 5
DUSP6	dual-specificity MAPK phosphatase 6
EBI2	Epstein-Barr virus-induced gene receptor 2
EBOV	Ebola virus
ECL	enhanced chemiluminescence
ECM	extracellular matrix
EGF	epidermal growth factor
EGFR	epidermal growth factor receptor
ER	endoplasmic reticulum
ERK	extracellular signal-regulated kinase

ERα	estrogen receptor-α
FAK	focal adhesion kinase
FAT1	FAT atypical cadherin 1
FBS	fetal bovine serum
GAPDH	glyceraldehyde-3-phosphate dehydrogenase
GEF	guanine nucleotide exchange factor
H_2O_2	hydrogen peroxide
HAEC	human aortic endothelial cell
HB-EGF	heparin-binding EGF-like growth factor
HIF1α	hypoxia-inducible factor 1α
HIV	human immunodeficiency virus
HMG-CoA	3-hydroxy-3-methylglutaryl Coenzyme A
HRP	horseradish peroxidase
IC	intracellular
ICAM-1	intercellular adhesion molecule 1
IFN	interferon
IGF-1R	insulin-like growth factor-1 receptor
IgG	immunoglobulin G
IL-1β	interleukin-1β
IL-6	interleukin-6
IL-8	interleukin-8
IN-8	JNK-IN-8
iNOS	inducible NO synthase
IP_3	inositol 1,4,5-trisphosphate
Insig	insulin induced gene protein
JAK	Janus kinase
JNK	c-Jun N-terminal kinase
KLF4	Krüppel-like factor 4
LB	Luria Broth
LC-MS/MS	Liquid Chromatography–Tandem Mass Spectrometry
LDL	low density lipoprotein
LPS	lipopolysaccharides
LXR	liver X receptor
MAPK	mitogen-activated protein kinase
MCP-1	monocyte chemoattractant protein-1
MEK	mitogen-activated protein kinase kinase
MERS-CoV	Middle East respiratory syndrome coronavirus

MKP-1	MAPK phosphatase-1
MMP	matrix metalloproteinase
MMP-2	matrix metalloproteinase 2
MMP-9	matrix metalloproteinase 9
mRNA	messenger ribonucleic acid
NAD(P)H	nicotinamide adenine dinucleotide phosphate
NF-κB	nuclear factor kappa-B
NiV	Nipah virus
NO	nitrogen monoxide
Nox	NA(P)DH oxidase
O_2^-	superoxide
OH	hydroxyl group
oxLDL	oxidized low density lipoprotein
p38 MAPK	p38 mitogen-activated protein kinase
PBS	phosphate-buffered saline
PCC	Pearson's correlation coefficient
PCR	polymerase chain reaction
PDGFβ-R	platelet-derived growth factor β receptor
PFA	paraformaldehyde
PI3-K	phosphoinositide 3-kinase
PIP3	phosphatidylinositol-3,4,5-triphosphate
PKA	protein kinase A
PKC	protein kinase C
PLC	phospholipase C
PVDF	polyvinylidene difluoride
qRT-PCR	quantitative real-time PCR
RAAS	renin-angiotensin-aldosterone system
RNA	ribonucleic acid
ROR	receptor-related orphan receptor
ROS	reactive oxygen species
Runx2	runt-related transcription factor 2
SAC1	phosphatidylinositol-3-phosphatase
SARS-CoV-2	severe acute respiratory syndrome coronavirus 2
Scap	SREBP cleavage activating protein
Ser	serine
SR	sarcoplasmic reticulum
SREBP	sterol regulatory element binding protein

STAT	signal transducer and activator of transcription
TBS	tris-buffered saline
TEMED	tetramethylethylenediamine
TGF-β	transforming growth factor β
Thr	threonine
TIMP	tissue inhibitor of metalloproteinase
TLR	Toll-like receptor
TNF-a	tumor necrosis factor alpha
TRV3	TRV120023
Tyr	tyrosine
VCAM-1	vascular cell adhesion molecule 1
VSMC	vascular smooth muscle cell
VSV	vesicular stomatitis virus
ZIKV	Zika virus

1. Introduction

1.1. Overview

Presently, cardiovascular diseases (CVD) put an enormous burden on the healthcare system and remain the most common cause of death. Amongst the risk factors of CVDs, we find dietary and lifestyle choices. However, aging and the disruption of physiological regulatory processes also play a key part in the development of CVDs. One of the major endocrine mediators of vascular functions is angiotensin II (AngII), the vasoactive effector peptide hormone of the renin-angiotensin-aldosterone system (RAAS). Physiologically, AngII is responsible for vasoconstriction of resistance arteries through its type 1- AngII receptor (AT1R) on the surface of vascular smooth muscle cells (VSMC). Problems arise when RAAS is hyperactive. Exaggerated AngII effects lead to hypertrophy, remodeling, and inflammation in the vessel wall. These adverse effects are important steps in the pathogenesis of atherosclerosis - a complex inflammatory pathology of the vasculature - and result from the multifaceted signaling through the AT1 receptor. AT1R activity leads to diverse cell responses, including the transactivation of growth receptors and changes in gene expression.

In order to mechanistically understand the long-term effects of AngII and AT1R signaling in the vasculature, it is crucial to explore the gene expression changes caused by the hormone stimulus. The subject of this thesis, thus, is the study of the signaling pathway originating from the AT1R that promotes the upregulation of an oxysterol-producing enzyme, the expression of which was not described in the VSMCs previously. To provide background information on the subject of my thesis, the introduction covers AngII-induced signaling and its involvement in CVD development, as well as the characteristics of the oxysterols, their function, and their effects on vascular pathology.

1.2. The renin-angiotensin-aldosterone system

The renin-angiotensin-aldosterone system (RAAS) is an important endocrine system coordinating fundamental physiological processes. The RAAS regulates extracellular fluid volume and arterial blood pressure thus influencing cardiovascular and renal functions. Stimuli activating RAAS include decreased arterial blood pressure and sodium-chloride level, as well as sympathetic nervous system activity [1]. The system consists of enzymes and hormones that enact their respective effects at different organ sites. Upon RAAS activation, initially, renin is synthesized and secreted by the juxtaglomerular cells

in the kidney. The product of the renin gene is an inactive peptide, the preprorenin. Proteolytic cleavage of preprorenin and the subsequently generated prorenin leads to the formation of the enzymatically active renin [2]. Renin released from the cells cleaves angiotensinogen in the bloodstream to produce angiotensin I (AngI). AngI is further lysed by angiotensin converting enzyme (ACE) - located on the surface of endothelial cells in the lung capillaries - into angiotensin II (AngII), the octapeptide effector hormone of the RAAS. AngII promotes both vasoconstriction, which elevates blood pressure, and aldosterone synthesis in the adrenal gland cortex, resulting in increased Na^{1+} reabsorption in the proximal tubules. Thus, it is responsible for the major RAAS effects **(Figure 1)** [1].

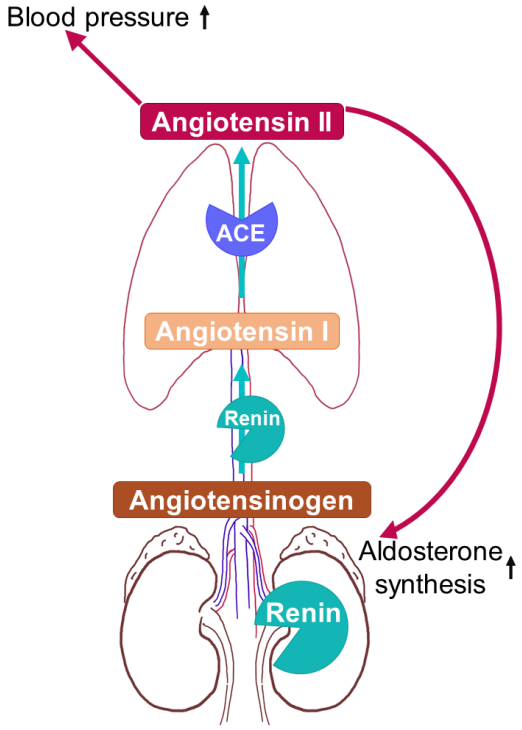

Figure 1. Mechanisms and functions of renin-angiotensin-aldosterone system (RAAS). The image represents the function of renin, angiotensin converting enzyme (ACE), and angiotensin II (AngII) in the RAAS. Renin is produced in the kidneys, and it catalyzes the cleavage of angiotensinogen into angiotensin I. The ACE will then convert Angiotensin I into AngII in the lungs. Turquoise arrows indicate the enzymatic actions leading to AngII production, whereas red arrows show the endocrine effects of AngII. (Own figure based on the first paragraph of chapter 1.2.)

In addition to the systemic RAAS with its endocrine effects, there is evidence of locally working RAAS in various tissues. In the heart, vascular tissue, kidney, and the brain components of RAAS are expressed or taken up from the plasma, allowing the locally synthesized AngII to affect the functions of these organs independently from the

circulating angiotensins [3]. The cardiac RAAS is activated during heart failure, where renin is either sourced from the plasma or is expressed by cardiac cells, in which case it is not secreted, rather, it remains intracellularly and enacts a cardioprotective role [4–6]. The RAAS in the heart affects cell communication via the intracellular effects of its components [6]. The intrarenal RAAS regulates the excretory functions. In the kidney, AngII distribution varies between the cortex and medulla. The locally generated AngII constricts glomerular arterioles, influencing renal medullary blood flow and eventually the renal hemodynamics. Moreover, AngII directly promotes tubular reabsorption of sodium [7]. Besides the above mentioned major organs, adipose tissue can also express angiotensinogen, renin, and ACE. It was found that obesity contributes to elevated AngII production in the adipose tissue [3]. Literature data highlights the functional roles of local RAAS components, especially under pathological conditions of the affected organ.

1.3. AngII-induced signaling in vascular smooth muscle cells

1.3.1. $G_{q/11}$-protein related signaling

The vascular smooth muscle cell (VSMC) is a prominent effector cell of the AngII. VSMCs are an essential component of vessel walls, and their physiology is intertwined with the sufficient functions of vessels. The classical effect of AngII on the vasculature is vasoconstriction. AngII activates the AT1R, a G-protein coupled 7 transmembrane receptor found on the surface of VSMCs. The agonist-receptor interaction activates $G_{q/11}$, which leads to the production of diacylglycerol (DAG) and inositol 1,4,5-trisphosphate (IP_3) by the enzyme phospholipase C (PLC). DAG promotes protein kinase C (PKC) activation, while IP_3 binds the IP_3 receptor, thus causing the release of calcium ions from the sarcoplasmic reticulum (SR). The elevated intracellular (IC) calcium level results in VSMC contraction, consequently vasoconstriction **(Figure 2)** [8]. PKC can also contribute to a continued smooth muscle contraction by phosphorylating a myosin light chain phosphatase inhibitor, the protein phosphatase 1 regulatory subunit 14 (CPI-17) and actin-binding proteins - calponin, calmodulin - thus increasing actin-myosin interaction [9]. A sustained agonist stimulus results in AT1R desensitization, in which process PKC plays a role by phosphorylating serine residues at the C-terminus of the receptor [10–12]. G-protein receptor kinases function similarly, by phosphorylation of the C-terminus, they enable desensitization. The phosphorylation signal on AT1R recruits β-arrestin proteins that promote receptor internalization.

Following the receptor internalization, multiple events may occur. Receptors may be recycled to the membrane, degraded or a new signaling event may be initiated by β-arrestins. β-arrestins can act as adaptor proteins. In this way, they play a role in mitogen-activated protein kinase (MAPK) and phosphoinositide 3-kinase (PI3-K) activation. As it stands, activated AT1R induces both G-protein and β-arrestin functions. This phenomenon opens up opportunities during drug development. Biased, functional selective, AT1R agonists have been developed, these biased ligands - e.g. TRV027; TRV023; SII-AngII - are able to trigger either G-protein or β-arrestin dependent signaling [13,14].

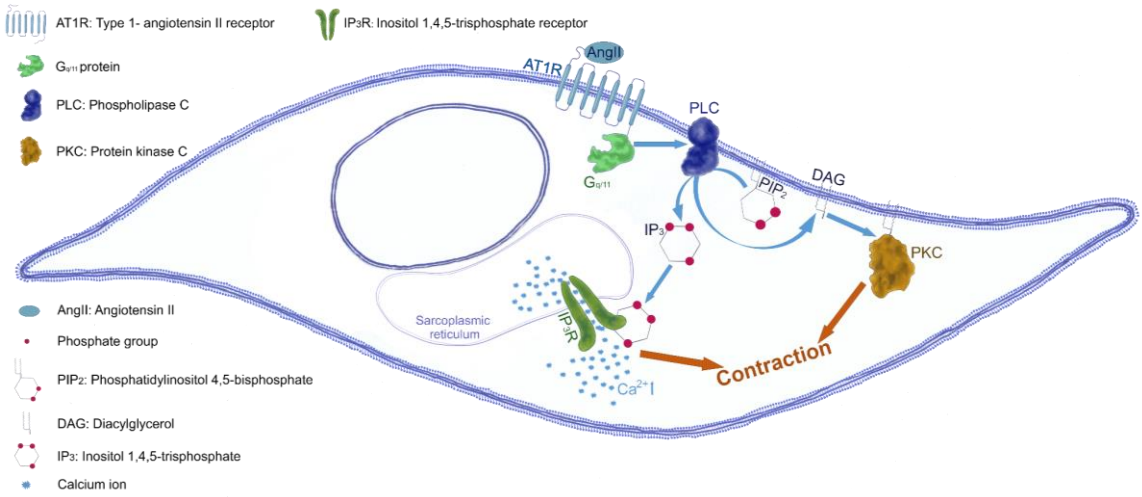

Figure 2. Effects of AngII-induced AT1R signaling through $G_{q/11}$ in smooth muscle cell function. Blue arrows represent promoting actions between the actors in the signaling pathway, whereas orange arrows indicate the resulting cellular response. (Own figure, based on chapter 1.3.1.)

1.3.2. Growth factor receptor transactivation and the activation of mitogen-activated protein kinase pathway

However, the effects of AngII reach beyond the conventional $G_{q/11}$-mediated events due to the aforementioned complexities of AT1R signaling. AT1R activation triggers multifaceted cellular responses thanks to its ability to transactivate other major signaling pathways, most notably growth factor receptor-related pathways [8]. Studies focusing on AT1R related receptor transactivation date back to the 1990s. It was shown that AngII promotes the activation and phosphorylation of the insulin-like growth factor-1 receptor (IGF-1R), whose phosphorylation is dependent on c-Src activation [15,16]. It was recognized decades ago that AngII activates various MAPKs, too, through epidermal

growth factor (EGF) receptor (EGFR) transactivation. EGFR transactivation is achieved by the AngII-induced calcium signal as well as via a metalloprotease-dependent mechanism [17–19]. In the latter case, AngII stimulus leads to the cleavage of heparin-binding EGF-like growth factor (HB-EGF) by a disintegrin and metalloprotease 17 (ADAM17) protein [20]. HB-EGF then acts as a ligand for EGFR, and subsequently, p38 MAPK and extracellular signal-regulated kinase (ERK) are activated in VSMCs [19]. It has been known for decades that AngII activates nicotinamide adenine dinucleotide phosphate (NAD(P)H) oxidase, thus induces reactive oxygen species (ROS) generation in VSMCs, partially due to phosphatidic acid accumulation during the hormonal stimulus [21]. Interestingly, it was found that EGFR transactivation, following AngII stimulus, plays a role in NAD(P)H oxidase activity. In this way, EGFR mediates multiple cellular responses promoted by AngII [22]. ROS generation enables AngII to activate other growth-related signaling events. AngII activates p38 MAPK in a redox-sensitive manner on account of its H_2O_2 production-promoting effect in VSMCs [23]. The platelet-derived growth factor β receptor (PDGFβ-R) is also phosphorylated upon AngII stimulus in VSMCs [24]. The AngII-induced activation of PDGFβ-R relies on Shc adaptor protein phosphorylation and ROS but is entirely independent of AT1R-generated calcium signal [25]. By virtue of its ability to activate these growth-promoting signaling pathways AngII contributes to mitogenic processes and hypertrophy **(Figure 3)** [23].

1.3.3. AngII-induced gene expression changes

Not surprisingly, the crosstalk between AT1R and growth receptors results in gene expression changes. Oftentimes, these changes lead to proliferative and phenotypic consequences. Notably, AngII induces the expression of c-fos, c-jun, and c-myc, which demonstrates its role in VSMC growth and hypertrophy [26–28]. Additionally, AngII can stimulate the Janus kinase (JAK)/signal transducer and activator of transcription (STAT) pathway, which is involved in inflammatory responses. The phosphorylation of STAT1 and STAT2 indicates that AngII contributes to the activation of cytokine-related pathways [29]. It was found that AngII-induced proliferation of VSMCs relies on the activity of STAT3 and ERK1 [30]. STAT proteins are also mediators of VSMC phenotype. For example STAT1 transcription factor promotes VSMC dedifferentiation, a prominent process in vascular remodeling [31]. Vascular remodeling is further characterized by the increased migratory capacity of VSMCs and an inflammatory state of the tissue, which is

associated with a marked up immune cell infiltration. AngII is responsible for such gene expression changes that enable these processes. VSMC migration is regulated by several proteins, including an atypical cadherin called FAT atypical cadherin 1 (FAT1). It was shown that AngII upregulates both FAT1 and a NA(P)DH oxidase (Nox) enzyme, the Nox1 expression in VSMCs. Bruder-Nascimento *et al.* in their study highlighted the significance of AngII-induced ROS generation through the Nox1 enzyme and subsequent ERK activation in the upregulation of FAT1. They observed that VSMC migration was inhibited by an antioxidant agent, AT1R antagonist, or FAT1 knockdown. As evidenced by their results, VSMC migration in response to AngII stimulus requires the FAT1 protein, the expression of which is AT1R-, and ROS-dependent [32]. AngII is also known to promote macrophage infiltration in the vessel wall, largely by its ability to upregulate chemokine expression, such as monocyte chemoattractant protein-1 (MCP-1) [33]. A recent study by Dan Qi *et al.* provided insight into this AngII-mediated phenomenon. They found that AngII upregulates the expression of hypoxia-inducible factor 1α (HIF1α) in VSMCs both *in vivo* and *in vitro*. The HIF1α deficiency in VSMCs leads to decreased AngII-induced cytokine and chemokine production, which ultimately reduces macrophage infiltration and vascular remodeling [34]. AngII not only regulates gene expression on its own, but it can also influence expression changes exerted by other factors. Initially, it was observed that AngII inhibits the interleukin-1β (IL-1β)-induced inducible NO synthase (iNOS) expression in VSMCs. This effect of AngII was attributed to the transient ERK phosphorylation detected when both AngII and IL-1β stimuli were utilized compared to the sustained ERK activation when only IL-1β stimulus was applied. The role of p38 MAPK activation by AngII was noted in this modified ERK signal [35]. Later, it was found that AngII upregulated the MAPK phosphatase-1 (MKP-1) - a negative regulator of MAPK action - in a p38 MAPK-dependent manner. This negative feedback contributes to the transient ERK activation seen during AngII stimulus [36]. Interestingly, this is not the only evidence of AngII-induced upregulation of MAPK regulators. AngII induces the gene expression of several dual-specificity MAPK phosphatases (DUSPs) in VSMCs, according to a recent report by our group [37]. Apparently, AngII modulates MAPK activity through the gene expression modulation of phosphatases and thus achieves tuning of MAPK-mediated cellular responses.

These findings clearly establish the gene expression-modulating role of AngII, which is achieved by its ability to trigger and transactivate several unrelated signaling pathways. Moreover, these AngII-induced gene expression changes prompt cellular responses, which largely influence vascular pathology thus their importance cannot be overstated. However, the understanding of AngII-induced gene expression changes and how these genes contribute to VSMC physiology and pathophysiology is still incomplete.

1.3.4. AngII-induced ROS generation

Similarly to other cell types, VSMC NAD(P)H oxidase consists of several subunits, the p22phox, p47phox, and catalytic subunits such as Nox1 or Nox4. For NAD(P)H oxidase activation small G proteins like Rac are needed [22]. AngII-induced ROS generation in VSMCs is the consequence of multiple pathways. ROS production can be the result of phospholipase D (PLD) activation upon AngII stimulus. PLD activation was shown to be associated with superoxide (O_2^-) production in VSMCs [38]. Additionally, the PLD enzyme produces phosphatidic acid (PA), a known activator of NAD(P)H oxidases. PA accumulation in VSMCs leads to a sustained activity of NAD(P)H oxidases and thus a long-term ROS production that lasts up to 6 hours [21]. ROS generation induced by AngII is a two-phase process. Initially, a rapid but moderate ROS generation - peaking at 30 seconds - occurs, which depends on PKC activity **(Figure 3)**. Approximately 30 minutes into the AngII stimulus, ROS production in VSMCs steadily increases and then lasts for 4-6 hours. The redox burst of the first phase enables c-Src activation and subsequent EGFR activation. EGFR then activates PI3-K and the PI3-K product phosphatidylinositol-3,4,5-triphosphate (PIP3) enhances Rac-guanine nucleotide exchange factor (GEF) resulting in elevated Rac activity that contributes to a sustained ROS production by NAD(P)H oxidase [21,22]. The role of c-Src in AngII-induced ROS generation is considered to be multifaceted. There is evidence that c-Src phosphorylates the p47phox subunit of NAD(P)H oxidase. This phosphorylation event is needed for the membrane translocation of p47phox, complex formation, and enzyme activation [39]. AngII induces both superoxide (O_2^-) and hydrogen peroxide (H_2O_2) but there is a distinction between the enzymes that produce these two ROS forms. Nox4 is responsible for the basal H_2O_2 formation in VSMCs and Nox4 depletion does not affect AngII-induced O_2^- production. In contrast, Nox1 enzyme produces O_2^-. Interestingly, in the absence of Nox1 AngII cannot induce either O_2^- or H_2O_2 but basal H_2O_2 levels are not

affected, which suggests that O_2^- produced by Nox1 - at least in part - is dismutated into H_2O_2 during AngII stimulus [40].

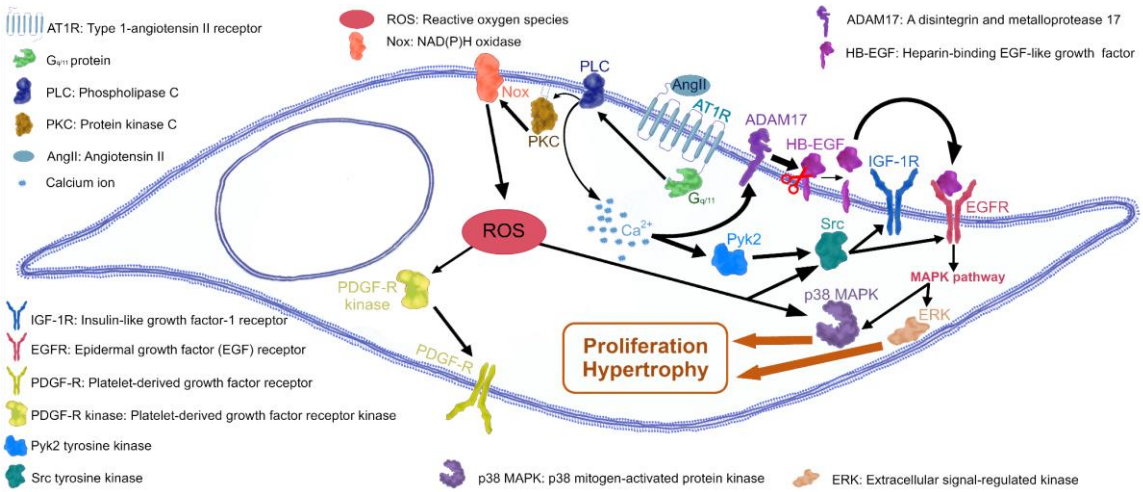

Figure 3. Scheme of growth pathway activation and ROS production induced by AngII. Black arrows represent promoting actions between the actors of the various signaling pathways whereas orange arrows indicate the resulting cellular responses. The red scissor signifies cleavage by ADAM17 enzyme. (Own figure based on chapters 1.3.2. and 1.3.4.)

1.4. AngII and cardiovascular pathologies

As alluded to previously, AngII is involved in a number of cardiovascular pathologies. This in part is due to its growth-promoting tendencies. The increased proliferation and growth lead to hyperplasia and hypertrophy respectively, which translates to thickening and vascular remodeling at the tissue level. These structural changes increase vessel stiffness, contributing to atherosclerosis and hypertension [41,42]. ROS production caused by AngII is a prominent player in hypertrophy [21,43,44]. Unsurprisingly, c-Src is also involved in AngII-induced VSMC hypertrophy and proliferation since this kinase participates both in the IGF-1R and NAD(P)H oxidase activation [16,22,39]. Cardiomyocytes are also affected by AngII-induced hypertrophy as a consequence of EGFR transactivation upon AngII stimulus [45].

Atherosclerosis is a complex inflammatory pathology of the vasculature, accompanied by endothelial injury and local lipid accumulation. Endothelial dysfunction enables the infiltration of low density lipoprotein (LDL) and immune cells. Lipid accumulation is a prominent step in atheromatous plaque formation. The macrophages take up LDL and other lipids, which in turn promotes the transformation of macrophages into foam cells. Cytokines, growth factors, and ROS production in the plaque lead to VSMC dedifferentiation and migration, eventually a fibrous cap is formed consisting of

migrated VSMCs and extracellular matrix (ECM) components. However, ROS promotes matrix metalloproteinases (MMP) release. As a result, MMPs can break down the ECM proteins in the fibrous cap. This process decreases plaque stability and leads to lesion rupture, which may cause arterial thrombosis [46,47].

The molecular mechanism of atherosclerotic plaque formation is affected by AngII. Endothelial dysfunction caused by ROS can be traced back to AngII-induced actions. Furthermore, AngII upregulates vascular cell adhesion molecule 1 (VCAM-1) and intercellular adhesion molecule 1 (ICAM-1) expression in endothelial cells, the monocyte chemoattractant protein-1 (MCP-1) is also upregulated by the hormone. These processes result in a pronounced monocyte infiltration into the vessel tissue [33,47]. Inflammation is further promoted by the AngII-induced upregulation of interleukin-6 (IL-6), tumor necrosis factor alpha (TNF-a), and nuclear factor kappa-B (NF-κB). AngII enables vascular remodeling, not only by promoting VSMC proliferation and migration but also by stimulating collagen synthesis thus inducing fibrosis [47–50]. The effect of these pathological changes is the development of hypertension, a condition that has an adverse effect on heart function since it promotes left ventricular hypertrophy and heart failure [51,52].

1.5. Introduction to an oxysterol: the generation and functions of 25-hydroxycholesterol

The widely studied 25-hydroxycholesterol (25-HC) is an oxysterol. Oxysterols are the oxidation derivatives of cholesterol. Their production is either the result of enzymatic or non-enzymatic reactions, where the enzymatic oxidation mainly occurs on the cholesterol side chain [53,54]. In some cases, the oxysterol may be formed by either reaction. For example, 25-HC may also be generated by free radical attack of cholesterol. However, this reaction has little importance *in vivo*, the endogenously produced 25-HC primarily originates from the action of cholesterol-25-hydroxylase (CH25H) enzyme **(Figure 4)** [55]. Oxysterols are a vast group of lipid molecules that are considered both metabolites - since they are intermediates in steroid hormone and bile acid synthesis - and bioactive lipids. Oxysterols meet the criteria of metabolites, as they are structurally similar to cholesterol, produced intracellularly, processed by enzymes, they act as substrates in subsequent reactions, and do not accumulate in the cells. At the same time the majority of oxysterols are bioactive and exert regulatory functions in the cholesterol

and lipid metabolism. Furthermore, they have specific targets, bind receptors, and thus impact cellular functions, but most importantly oxysterol level altercation influences pathology [56].

Oxysterols target both the cholesterol biosynthesis pathway and cholesterol efflux. 25-HC was first recognized as a regulator of sterol synthesis, as it inhibits 3-hydroxy-3-methylglutaryl Coenzyme A (HMG-CoA) reductase. In this way, 25-HC interferes with the rate-limiting step of cholesterol synthesis [57]. 25-HC further inhibits cholesterol synthesis through the sterol regulatory element binding protein (SREBP), a transcription factor necessary for the expression of enzymes in the cholesterol synthesis. It was shown that 25-HC suppresses SREBP cleavage by binding to insulin induced gene protein (Insig) thus, 25-HC promotes the interaction between Insig and SREBP cleavage activating protein (Scap), which prevents SREBP activation [58,59]. Oxysterols also act as ligands for liver X receptors (LXR). LXR activation leads to the expression of ATP-binding cassette transporters (ABC) involved in cholesterol efflux [56,60].

Oxysterols target specific receptors. They bind retinoic acid receptor-related orphan receptors (ROR), which are activators of transcription [56]. 25-HC is a ligand for estrogen receptor-α (ERα) and is able to activate the receptor in cancer cells and cardiomyocytes [61]. The Epstein-Barr virus-induced gene receptor 2 (EBI2) is activated by 7α,25-Dihydroxycholesterol (7α,25-OHC), a metabolite of 25-HC. EBI2 activates the migration of B cells and dendritic cells, this is one of the sites where 25-HC can mediate immune functions [55,56,62,63]. 25-HC also binds integrins α5β1 and αvβ3 in macrophages, as a result, focal adhesion kinase (FAK) is phosphorylated and activated [64].

25-HC is a potent lipid in immunological processes, it mediates not only innate immune responses but also acts as an antiviral agent during virus infections. The expression of CH25H is prominent in macrophages and dendritic cells. *Ch25h* is an interferon-stimulated gene. It is upregulated in immune cells in response to lipopolysaccharides (LPS) stimuli, Toll-like receptor (TLR) activation, and LXR activation by 25-HC [65–67]. The subsequent 25-HC production observed in macrophages leads to the inhibition of IgA class switching in B cells thus 25-HC regulates interactions between the innate and adaptive immune system [68]. 25-HC induces interleukin-8 (IL-8), IL-6, and TNF expression in macrophages, promoting proinflammatory responses [64,69,70].

25-HC possesses strong antiviral effects due to the inhibition of viral entry which was demonstrated in the case of multiple viruses: vesicular stomatitis virus (VSV), human immunodeficiency virus (HIV), Nipah virus (NiV), Ebola virus (EBOV), and Zika virus (ZIKV) severe acute respiratory syndrome coronavirus 2 (SARS-CoV-2), SARS-CoV, and Middle East respiratory syndrome coronavirus (MERS-CoV) [71–73]. It seems that the inhibition of viral entry is a result of cholesterol depletion in the plasma membrane exerted by 25-HC [73].

Studies investigating macrophages provide ample data on the gene expression regulation of *Ch25h*. Over the years, numerous signaling pathways and transcription factors have been implicated in *Ch25h* expression. TLR-mediated upregulation of *Ch25h* seems to be dependent on p38 MAPK, c-Jun N-terminal kinase (JNK) activity, and the transcription factor NF-κB [68]. Additionally, *Ch25h* upregulation has been linked to the activity of STAT1, activating transcription factor-2 (ATF2) and Krüppel-like factor 4 (KLF4) transcription factors [60,74,75].

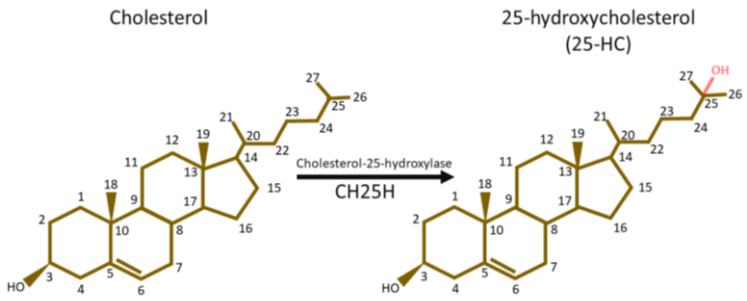

Figure 4. Structure and generation of 25-HC. The CH25H enzyme catalyzes the placement of a hydroxyl group (OH) onto the twenty fifth position of the cholesterol sidechain, creating an oxidized form of the molecule, the 25-HC. (Own figure)

1.6. Oxysterols in vascular pathology

Oxysterols play a significant role in vascular aging and atherosclerosis pathogenesis. Atherogenesis is characterized by the dysfunction of endothelial cells, inflammation, disrupted ECM structure, VSMC dedifferentiation, and apoptosis. Oxysterols are heavily involved in the process at every step of the way [76,77].

By the 1990s it was already known that cholesterol oxidation products are present in the aortic tissue, as evidenced by a study conducted on hypercholesterolemic rabbits [78]. Commonly found oxysterols in atherosclerotic regions include 25-HC, 27-HC, 7-ketocholesterol (7-K), and 7β-HC [76]. As for the source of oxysterols in the vessel wall,

oxidized LDL (oxLDL) must be highlighted - LDL accumulated in the vascular tissue undergoes oxidation - as well as immune cells that produce 25-HC through enzymatic process [77,79]. Similarly to AngII, oxysterols contribute to endothelial dysfunction via oxidative stress and altered adhesion molecule expression. Notably, 25-HC promotes VCAM-1 expression in human aortic endothelial cells (HAECs) [80]. This leads to an increased endothelial permeability, which favors monocyte infiltration. Additionally, oxysterols reduce nitrogen monoxide (NO) production of endothelial cells, which impairs sufficient vasodilatation capabilities [77].

Oxysterols promote the recruitment of immune cells by upregulating important chemokins such as IL-8 or MCP-1 [69,70,81]. It should be noted that in this respect too, the effects of oxysterols are very similar to those of AngII. Once monocytes infiltrate the vascular tissue, they differentiate into macrophages and contribute to the onset of inflammation. Moreover, oxysterols such as 25-HC promote proinflammatory gene expression in macrophages [64,79]. Macrophages take up the accumulated lipids and oxLDLs in the vascular tissue and then undergo transformation into foam cells. This inflammatory state enables the continuation of a downward spiral toward advanced atherosclerotic plaque formation [77].

The ECM possesses a pronounced importance in vascular pathology. During atherogenesis, excessive collagen deposition facilitates vascular stiffness and the progression of fibrosis. Transforming growth factor β (TGF-β) is one of the key cytokines that drive profibrotic events. TGF-β activates fibroblasts, upregulates type I collagen expression and hinders MMP action by stimulating tissue inhibitor of metalloproteinase (TIMPs) production [82]. Oxysterols were shown to upregulate TGF-β expression in macrophages [83]. In this way, oxysterols add to the formation of the fibrous cap, which consists of ECM proteins and VSMCs, a structure that surrounds the lipid core of the plaque. However, oxysterol actions during the pathogenesis of atherosclerosis vary as the lesion progresses. It is suspected that the amount of accumulated oxysterols in the plaque influences their effects on the atherosclerotic process. Oxysterol accumulation over time is enhanced thus their effects are increasingly deleterious [77]. The oxysterols 27-HC and 7α-HC upregulate MMP-9 expression in macrophages in a ROS-dependent manner. This finding suggests that oxysterols also endanger plaque stability, as MMPs degrade ECM,

weakening the fibrous cap and thus enhancing the risk of plaque rupture and thrombus formation [84].

However, MMPs are also significant at earlier stages of plaque progression and their activity actually helps fibrous cap formation initially. MMP-2 fosters VSMC migration by breaking down type IV collagen and laminin, which allows VSMC detachment from ECM. Additionally, growth factors are released during ECM degradation [85]. The 7-K and cholesterol-5α,6α-epoxide (α-epoxide) oxysterols promote VSMC migration due to the upregulation of MMP-2 and MMP-9 and the activation of the EGFR/PI3-K/Akt pathway. Not only that, but 7-K and α-epoxide also promoted VSMC proliferation at low concentrations (2.5 μM). It is important to note that the same oxysterols exert cytotoxic effects and decrease cell viability at high concentrations (25 μM - 50 μM) [86]. These data support the idea that differing oxysterol quantities influence atherogenesis in distinct ways. Ultimately, VSMCs proliferate, undergo phenotypic change, and migrate from tunica media to tunica intima, contributing to fibrous cap formation [77].

As mentioned, the stability of the atherosclerotic plaque depends on the structure of the fibrous cap. Besides MMPs apoptosis of VSMCs also destabilizes the plaque. Oxysterols, particularly at high concentrations, promote apoptosis of VSMC. As early as 1988 Cox *et al.* reported that 25-HC promoted cell death of rabbit thoracic aorta VSMC culture [87]. In later years the underlying mechanisms were being investigated. It was found that 25-HC and 7-K downregulated Bcl-2 - an antiapoptotic protein - expression in rabbit aortic VSMCs [88]. Another hallmark of 25-HC-induced VSMC apoptosis is the activation of caspase-3 protein, the cleavage of which was reported by a couple of studies [89,90]. 25-HC influences another Bcl-2 family protein, it activates the proapoptotic Bax protein, which is a major player in the mitochondrial pathway of apoptosis [90,91]. 25-HC contributes to soluble adenylyl cyclase activation thus the increasing cyclic adenosine monophosphate (cAMP) causes protein kinase A (PKA) activation. PKA phosphorylates Bax hence promoting its translocalisation to the mitochondria. The resulting ROS release and caspase activity leads to apoptosis in VSMCs [90]. It is worth mentioning that studies investigating the apoptotic effects of 25-HC employ high concentrations of oxysterol (~ 40-50 μM) and an incubation period of 24 hours. This supports the notion that the cytotoxic effects of oxysterols are prevalent when they are present in excessive amounts over a prolonged period [90–92].

Another prominent event of atherosclerotic plaque progression is calcification. VSMCs are especially prone to calcifying, resulting in the extreme stiffness of the vessel wall. Oxysterols, such as 25-HC, were shown to exert calcifying effects [93]. Cholestane-3β, 5α, 6β-triol (triol) causes calcification of rat VSMC culture *in vitro* in a dose-dependent manner and ROS was implicated as a mediator of the process [94]. 7-K-induced VSMC calcification is also dose-dependent. Furthermore, the enhanced calcium deposition is accompanied by the upregulation of bone-related genes, such as runt-related transcription factor 2 (Runx2) and osteopontin, which signifies the osteoblastic transition of VSMCs [95]. 25-HC was also reported to induce Runx2 upregulation in VSMCs. The calcification-inducing effect of 25-HC was attributed to inflammation and subsequent endoplasmic reticulum (ER) stress promoted by the oxysterol [96].

25-HC and other oxysterols have been shown to contribute to atherogenesis. However, their actual role in this pathogenesis remains controversial. There has been some evidence in the past that suggests an atheroprotective role of oxysterols. The clearance of subcutaneously implanted cholesterol tablets without oxysterols versus the clearance of cholesterol tablets containing oxysterols was studied in rats. The study found that oxysterol containing tablets exhibited enhanced clearance, suggesting the promotion of cholesterol solubilizing by oxysterols [97]. Later, accumulating evidence showed that oxysterols, which are ligands of LXR, are able to promote cholesterol efflux from macrophages. The functions of LXR are also linked to anti-inflammatory responses. Arguably, oxysterols display both proatherogenic and antiatherogenic capabilities and individual oxysterols affect vascular pathology in distinct ways [98]. In recent years, a study reported that $ApoE^{-/-}/Ch25h^{-/-}$ mice showed an increased lesion area in the thoracic aorta compared to $ApoE^{-/-}/Ch25h^{+/+}$, indicating an atheroprotective function of 25-HC [60]. Still, numerous studies report that 25-HC plays a significant role in vascular pathology and atherosclerotic plaque vulnerability on account of either paracrine signaling or cytotoxic effects [76,77,79,99]. Furthermore, a study investigating acute myocardial infarction biomarkers found CH25H to be a promising marker, as its expression is upregulated in patients compared to healthy subjects [100]. This highlights the importance of 25-HC and its functions in cardiovascular pathology. 25-HC-related actions have largely been the subject of studies investigating immune cell function in immunological and in atherosclerotic context. As for the source of 25-HC in the vessel

wall, its production by macrophages and the oxLDL have been highlighted. However, considering the major effects of 25-HC on the VSMCs, the similarities between 25-HC and AngII actions **(Figure 5)**, the fact that some AngII-induced effects were found to be mediated via 25-HC [101] it is compelling to explore the possibility of 25-HC production in VSMCs and underlying connections to AngII.

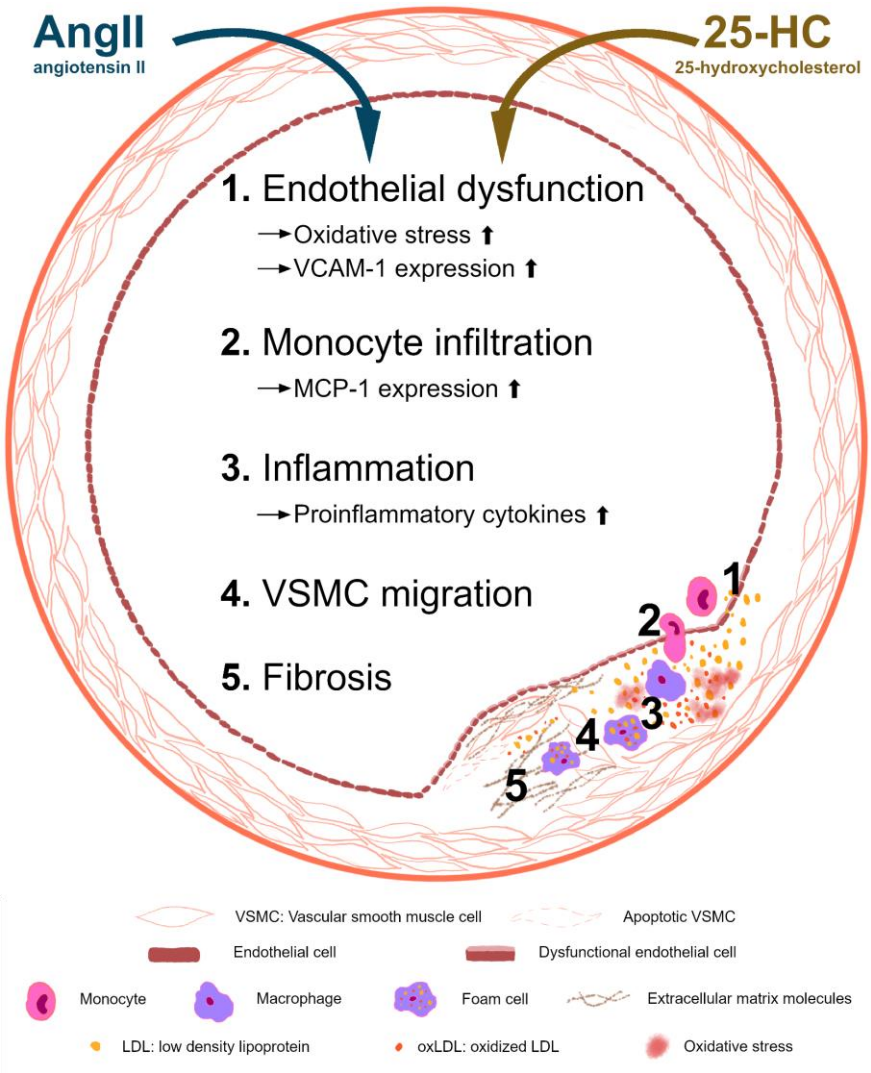

Figure 5: Summary of the atherogenic processes that are promoted by both AngII and 25-HC. The image represents a vessel wall with the scheme of atherogenesis in the lower right region. The numbered list includes atherogenic events - and some of their causes - that are promoted by both AngII (blue arrow) and 25-HC (brown arrow). Numbers in the image indicate the depiction of the given, listed atherogenic event. Abbreviations: VCAM-1: vascular cell adhesion molecule 1; MCP-1: monocyte chemoattractant protein 1; VSMC: vascular smooth muscle cell. (Own figure based on chapters 1.4. and 1.6.)

2. Objectives

This study aimed to characterize AngII-induced *Ch25h* expression in primary rat VSMCs isolated from the thoracic aorta. The objectives can be divided into two groups:

2.1. Investigation of AngII-induced *Ch25h* expression in VSMCs and underlying signaling pathways:

→Determination of the *Ch25h* messenger ribonucleic acid (mRNA) level changes in response to AngII stimulus and assessment of the time kinetics of the gene expression change.

→Defining the role of AT1R-related $G_{q/11}$ or β-arrestin signaling.

→Investigating and comparing the role of MAP kinase proteins in *Ch25h* and *Dusp* gene expression.

→Investigating the phosphorylation status of p38 MAPK and STAT1.

→Investigating the role of Nox activity.

2.2. Examination of CH25H activity in VSMCs:

→Verifying the subcellular localization of the CH25H enzyme.

→Assessing 25-HC levels in the supernatant of AngII-stimulated VSMC cultures.

3. Methods

3.1. Animals and isolation of primary rat VSMCs

The primary rat VSMCs used in our experiments originated from male Wistar rats (Charles River Laboratories-Semmelweis University, Budapest). Our laboratory follows the guidelines established by the Guide for the Care and Use of Laboratory Animals (NIH, 8th edition, 2011) and national legal and institutional guidelines for animal care. This study was approved by the Animal Care Committee of Semmelweis University, Budapest, and by Hungarian authorities (No. 001/2139–4/2012). All procedures followed legal and institutional guidelines for animal care.

VSMCs were isolated from male Wistar rats (170–250 g) aged 40-50 days. The animals were kept on a standard semisynthetic diet. VSMCs were isolated from the thoracic aorta according to the explant method described in an earlier study [102]. Following excision, the thoracic aorta was kept in modified Krebs-Ringer solution (120 mM NaCl (Duchefa Biochemie); 4.7 mM KCl (Duchefa Biochemie); 1.8 mM $CaCl_2$ (Duchefa Biochemie); 0.7mM $MgSO_4$ (Fluka); 10 mM glucose (Serva); and 10 mM Na-HEPES (Serva)) while branching arteries and tunica adventitia were removed. The prepared thoracic aorta was then sliced into 1 mm sized rings and incubated in collagenase (Collagenase type I., Worthington) for 25 minutes at 37 °C. These prepared aorta-rings were placed onto 10 cm cell culture plates (Greiner) in Dulbecco's modified Eagle media (DMEM High Glucose W/ L-Glutamine W/Sodium Pyruvate; Biosera) supplemented with 10% fetal bovine serum (FBS; Biosera), 1% penicillin–streptomycin (Sigma-Aldrich), and 1% GlutaMAX (Gibco). In order to promote VSMC growth, the aorta-rings were incubated at 5% CO_2 and 37 °C. The medium was replaced with fresh, supplemented DMEM the day after isolation of the thoracic aorta. Three days after the isolation, VSMCs were observable around the aorta-rings. At that point the aorta tissue was removed from the plates. Once VSMC cultures reached full confluence, they were passaged. For our experiments, VSMCs were used in the second and third passages.

3.2. Immunocytochemistry

Smooth muscle alpha-actin was immunostained to assess the homogeneity of primary VSMC cultures. During the immunolabeling procedure, the cells were kept on ice. VSMCs were washed with cold phosphate-buffered saline (PBS) between each step (137

mM NaCl; 2.7 mM KCl; 10 mM Na_2HPO4 (Sigma-Aldrich); 1.8 mM KH_2PO_4 (Fluka) in distilled water set to a pH value of 7.4). VSMCs were then fixed with 4% paraformaldehyde (PFA; Polysciences) for 15 minutes. For cell permeabilization, we used a 0.1% Triton X-100 (Sigma-Aldrich) solution for 5 minutes. VSMCs were then incubated in 0.1% sodium–borohydride (Sigma-Aldrich) solution for 15 minutes. The blocking step took place for 30 minutes, using a 1% bovine serum albumin (BSA; Sigma-Aldrich) solution. To label anti-smooth muscle alpha-actin, we used a monoclonal mouse primary antibody (A2547; Sigma-Aldrich) solution at a dilution of 1:500, the incubation lasted for 1 hour. VSMCs were then incubated in Alexa Fluor 488-conjugated anti-Mouse immunoglobulin G (IgG) secondary antibody (A-21200; Invitrogen) solution at a dilution of 1:300 for 30 minutes. Cell nuclei were labeled with TO-PRO3 nucleic acid stain (Thermo Fisher Scientific). Figure 6 shows representative images of our VSMC cultures where the smooth muscle alpha-actin (green) signal is consistent, and cell nuclei appear in blue.

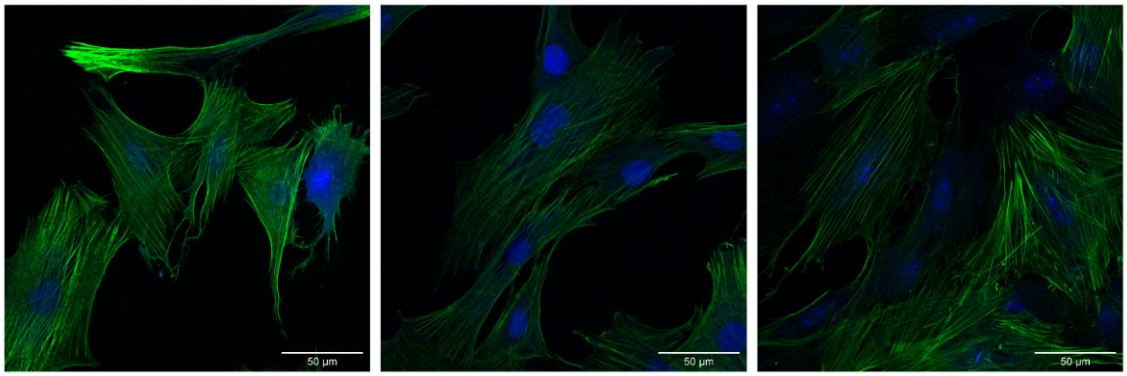

Figure 6. Smooth muscle alpha-actin signal in primary rat VSMC cultures. Smooth muscle alpha-actin (green) was immunolabeled in representative primary rat VSMC cultures. Cell nuclei (blue) are labeled with TO-PRO3 nucleic acid stain. Fixed cells were imaged using a Zeiss LSM 710 confocal microscope. Scale bars in white represent 50 µm. Source: Kovács KB *et al.* [103]

3.3. Stimulation of VSMCs

Prior to the experiments, we serum starved the primary VSMC cultures overnight, using serum-free DMEM supplemented with 0.1% BSA (Sigma-Aldrich). During the experiments, VSMCs remained in serum-free DMEM and all reagents used to treat and stimulate the cells were also diluted in serum-free DMEM.

We investigated the time kinetics of *Ch25h* mRNA expression by stimulating VSMCs for various timespans. VSMCs were stimulated with 100 nM AngII for 1, 2, 3, 4, 5, and

6 hours or not stimulated. We also investigated the effects of biased AT1R agonist stimulus on *Ch25h* mRNA levels. In this case, the VSMCs were stimulated with either vehicle or 3 μM TRV120023 (TRV3; Proteogenix) biased AT1R agonist for 1 hour. Samples of these experiments were then prepared for RNA extraction.

To determine changes in 25-HC levels in response to AngII stimulus, VSMCs were stimulated with 1 μM AngII for 2, 4, 8, 16, and 24 hours or not stimulated. We prepared duplicate samples during the course of the experiments. Following the hormone stimulus, the supernatants of VSMCs were collected and subjected to Liquid Chromatography–Tandem Mass Spectrometry (LC-MS/MS) measurement.

3.4. Inhibitor treatments and hormone stimulation of VSMCs

These experiments were initiated by overnight serum deprivation of the VSMC cultures, as described above in section 3.3..When investigating the actions of various proteins in signaling events leading to gene expression changes, VSMCs were pretreated with differing inhibitors before the hormone stimulus. Control groups received dimethyl sulfoxide (DMSO) vehicle pretreatment since the inhibitors used in these experiments were dissolved in DMSO. Other groups were pretreated with 10 μM candesartan, 50 μM SB202190, 20 μM PD98059, 5 μM DPI (Sigma-Aldrich), 1 μM JNK-IN-8 (IN-8; Selleckchem) or 1 μM YM-254890 (Wako Chemicals). Pretreatment lasted for 30 minutes. Then we stimulated cells with 100 nM AngII (Sigma-Aldrich) or vehicle for 1 hour in case of *Ch25h* mRNA detection and for 2 hours in case of *Dusp* mRNA detection. Samples were then prepared for RNA extraction.

3.5. RNA isolation and complementary deoxyribonucleic acid (cDNA) preparation

In order to isolate total RNA content of VSMC samples, the hormone stimulus was stopped by discarding the stimulating media and washing the cells twice with cold, sterile PBS. Total RNA was isolated using the RNeasy Plus Mini kit from Qiagen. Briefly, cells were washed off the culture plate and lysed with a mixture of lysis Buffer RLT and 70% ethanol. Lysed samples were then loaded onto the spin columns provided in the kit and centrifuged for 30 seconds at 8000 *rcf* and 4°C. Samples were then washed with RW1 and RPE buffers (provided in the kit) with the help of further centrifugation steps. RNA was eluted with RNase-free water. RNA concentrations were determined with a spectrophotometer (NanoDrop ND-1000) at 260 nm.

For cDNA preparation, we diluted RNA samples to a concentration of 0.1 μg/μl with RNase-free water. Reverse transcription was carried out with the RevertAid Reverse Transcription Kit (Thermo Fisher Scientific) according to the manufacturer's instructions. We added 1-1 μl oligo-dT to each RNA sample and they were subjected to hybridization in a polymerase chain reaction (PCR) equipment (Eppendorf; Mastercycler) providing a temperature of 70°C for 5 minutes. Next, RevertAid reverse polymerase was added to the samples alongside its 5x transcriptase buffer, Ribolock RNase inhibitor, and deoxynucleotide triphosphate (dNTP). cDNA synthesis took place at the following parameters: 1. T=42°C, 65 minutes; 2. T=70°C, 10 minutes. cDNA samples were then diluted with 80 μl RNase-free water and stored at -20°C.

3.6. Quantitative real-time PCR (qRT-PCR)

Quantitative real-time PCR (qRT-PCR) procedure was used to assess gene expression changes in our samples. qRT-PCR reactions were prepared using the SYBR Green Kit (LightCycler 480 SYBR Green I Master; Roche) according to the manufacturer's instructions. This system utilizes a hot start PCR reaction, meaning that the polymerase requires a high-temperature (95°C) preincubation period to be active. Fluorescent signals are generated with the nucleic acid stain SYBR Green I. Detailed parameters of the thermal cycling are as follows: pre-incubation at 95 °C for 5 minutes, followed by amplification; 45 cycles of 10 seconds at 95 °C, 5 seconds at 62 °C, and 15 seconds at 72 °C, melting curve; 5 seconds at 95 °C, 1 minute at 65 °C and 97 °C, and cooling 30 seconds at 40 °C.

For the assessment of gene expression of target genes, we employed relative quantification, where the mRNA level of target genes was compared to that of a reference gene. As a reference, we used the mRNA level of the housekeeping gene, glyceraldehyde-3-phosphate dehydrogenase (*Gapdh*). Target genes investigated in our samples were: *Ch25h*, *Dusp5*, *Dusp6*, *Dusp10*. qRT-PCR primers were obtained from Sigma-Aldrich, their sequences are listed in Table 1. The measurements were carried out with the LightCycler 480 instrument (Roche). The cycle threshold (Ct) was calculated with the second derivative method using LightCycler 480 Software. Fold ratios of gene expression were calculated as follows:

$$\text{Ratio} = E^{\Delta Ct\ target\ gene} / E^{\Delta Ct\ Gapdh}.$$

Table 1. qRT-PCR primer sequences.

Gene name	forward primer (5'→ 3')	reverse primer (5'→ 3')
Gapdh	CCTGCACCACCAACTGCTTAG	CAGTCTTCTGAGTGGCAGTGTGATG
Ch25h	GCGTTGGCTACCCAATACAT	GTGAGTGGACCACGGAAAGT
Dusp5	GGCAAGGTCCTGGTTCACTGT	GTTGGGAGAGACCACGCTCCT
Dusp6	ATCACTGGAGCCAAAACCTG	CGTTCATGGACAAGTTGAGC
Dusp10	GGCAAAGAACCCCTGGTATT	AGAAACAGGAAGGGCAGGAT

3.7. Western blot

Western blot procedure was used to detect phosphorylated forms of p38 MAPK and STAT1 proteins. Prior to the procedure VSMCs were serum deprived overnight. The next day VSMCs were pretreated with 50 µM SB202190 (Sigma-Aldrich) or 1 µM YM-254890 (Wako Chemicals) for 30 minutes. Control groups received DMSO pretreatment. VSMCs were then stimulated with a vehicle or 100 nM AngII stimulation solution (Sigma-Aldrich). Stimulation lasted for 10 minutes or 20 minutes. Following stimuli, VSMCs were lysed with 100 µl 2X Laemmli sample buffer (4% sodium dodecyl sulfate (SDS; SERVA); 20% glycerol (SERVA); 0.004% bromophenol blue (Sigma-Aldrich); 125 mM Tris-Cl, pH 6.8; 10% 2-mercaptoethanol (Gibco)). Samples were stored at -80 °C.

Sample preparation took place directly before the electrophoresis. Briefly, samples were incubated at 100 °C for 5 minutes and then centrifuged for 2 minutes at 4 °C. Western blot procedure was carried out using Bio-Rad instruments. To execute electrophoresis, 10 µl of each sample was loaded into 8% polyacrylamide gels (8% acrylamide (SERVA); 25% 1.5 M Tris buffer (SERVA); distilled water; 0.05% tetramethylethylenediamine (TEMED; Sigma-Aldrich); 0.2% ammonium persulfate (APS; SERVA)), the proteins were run at 100 V in electrophoresis buffer (25 mM Tris; 192 mM glycine; 0.1 % sodium dodecyl-sulfate (SDS) in distilled water). Proteins were then transferred onto a polyvinylidene difluoride (PVDF) membrane (Thermo Fisher Scientific) using a Trans-Blot Turbo Transfer system (Bio-Rad) and transfer buffer (25 mM Tris; 192 mM mg/ml glycine) containing 20% methanol.

The PVDF membranes were then blocked for one hour in a tris-buffered saline (TBS; 137 mM NaCl; 2.7 mM KCl; 25 mM Tris) buffer containing 50 mg/ml milk powder and

0.1% Tween-20 (Sigma-Aldrich). The same buffer was used to dilute primary antibodies of rabbit origin (Cell Signaling) at a 1:1000 ratio. Phospho-p38 MAPK (Thr180/Tyr182) (9211S; Cell Signaling) protein was labeled in samples that were stimulated with AngII for 10 minutes, whereas phospho-STAT1 (Ser727) (8826S; Cell Signaling) was labeled in samples stimulated with AngII for 20 minutes. Membranes were incubated in the primary antibody solutions at 4 °C overnight. Horseradish peroxidase (HRP) conjugated secondary antibody against rabbit IgG (7076S; Cell Signaling) was used to label both primary antibodies. GAPDH was labeled with an HRP-conjugated primary mouse antibody (51332S; Cell Signaling) and used as a reference protein. Membranes were briefly incubated (1 minute; room temperature) in enhanced chemiluminescence (ECL) reagent to develop signals (Western Lightning Chemiluminescence Reagent Plus, Perkin Elmer). Imaging was performed using the Azure 600 Western Blot Imaging System (azure biosystems).

3.8. DNA construct preparation and cloning

A DNA construct was created for the expression of Cerulean-labeled CH25H fusion protein (Cerulean-CH25H). As a first step, we produced the DNA insert to be built into the expression vector and which insert includes the open reading frame (ORF) region of the *Ch25h* gene. For the amplification of *Ch25h* ORF we used the cDNA of a VSMC sample that was stimulated with AngII (100 nM) for 1 hour. This proved to be a sufficient template, as the cDNA of *Ch25h* was present in increased amounts. PCR primer design included ATAT overhang sequence to ensure optimal polymerase function. Primer sequences (Sigma-Aldrich) used during *Ch25h* amplification are listed in Table 2.

Table 2. PCR primer sequences for amplification of *Ch25h* ORF.

forward primer (5'→ 3')	ATATATGGCCTGCCACAACGTTTCG
reverse primer (5'→ 3')	ATATAGTCTGTTTCTTCTTCTGGTTCAAGTG

The amplification reaction mix contained 40 µl distilled water, 5 µl 10x Buffer (Agilent), 1 µl template in 1:10 dilution, 1-1 µl forward and reverse primers, 1 µl dNTP, and 1 µl Pfu Turbo polymerase (Agilent). PCR conditions were as follows: T=95°C 3 minutes; 35 cycle of: T=95°C 30 seconds, T=54°C 30 seconds, T=68°C 2 minutes; T=68°C 7 minutes. The amplicon was then subjected to agarose (2%; SERVA) gel electrophoresis, where DNA was labeled with ethidium-bromide (Invitrogen) and was

purified with the GeneJet Gel Extraction Kit (Thermo Fisher Scientific). The purified *Ch25h* amplicon was further amplified using primers containing the necessary restriction enzyme sites, which enabled the insert delivery into the plasmid (Table 3.). The forward primer contained the EcoRI site (GAATTC), whereas the reverse primer contained the AgeI site (ACCGGT).

Table 3. PCR primer sequences for addition of restriction enzyme sites to *Ch25h* ORF.

forward primer (5'→ 3')	ATATGAATTCGCCACCATGGCCTGCCACAACGTTTCG
reverse primer (5'→ 3')	ATATACCGGTAGTCTGTTTCTTCTTCTGGTTC

PCR conditions were the same as previously described. The PCR product was electrophoresed and purified as detailed above. Both the purified amplicon and the pEYFP-N1-Cerulean (Clontech) plasmid backbone were then digested with EcoRI and AgeI restriction enzymes (Thermo Fisher Scientific) separately, according to the manufacturer's instructions. Namely, DNA - enzyme mixtures were incubated at 37°C for 1 hour. *Ch25h* insert and pEYFP-N1-Cerulean were then incubated together overnight at 16 °C with T4 ligase and T4 ligase buffer (Thermo Fisher Scientific).

The completed *Ch25h*-pEYFP-N1-Cerulean (Cerulean-CH25H) plasmid construct was transformed into NEB10 bacteria (BioLabs) for cloning. 1 µl of the plasmid construct was incubated with 20 µl of bacterial suspension for 30 minutes on ice followed by heat shock treatment at 42°C. The bacteria were then kept in Super Optimal broth with Catabolite repression medium (S.O.C.; Invitrogen) in a shaker for one hour at 37°C. The transformed bacteria were then centrifuged, the supernatant was removed. The bacteria were resuspended in 100 µl S.O.C. medium and spread onto Luria Broth (LB; Invitrogen) solid medium containing bacteriological agar (Biolab) and kanamycin (25 µl; 50 mg/ml; SERVA). Bacterial colonies appeared after overnight incubation at 37°C. Colonies were transferred to LB and kanamycin-containing liquid cultures (4 ml volume) and placed into a shaker overnight at 37°C. GeneJet Plasmid Miniprep Kit (Thermo Fisher Scientific) was used to isolate plasmid DNA. Plasmid DNA samples were then digested using EcoRI and AgeI. The digestion product was electrophoresed. The transformed NEB10 culture in which the pEYFP-N1-Cerulean backbone and *Ch25h* DNAs appeared separately and in the appropriate base pair region was deemed suitable for further culturing. Accordingly, the remaining bacteria were transferred into 150 ml of liquid culture medium (LB;

kanamycin) in order to obtain a sufficient amount of Cerulean-CH25H plasmid DNA. Following overnight incubation in a shaker at 37°C, plasmid DNA was isolated using the ZymoPURE II Plasmid Midiprep Kit (Zymoresearch) according to the manufacturer's instructions. The concentration of the Cerulean-CH25H DNA construct was measured with a NanoDrop ND-1000 device. The DNA construct was stored at 4°C.

The organelle marker (mRFP-SAC1; mRFP-TGN38; mRFP-Giantin) encoding DNA constructs used in this study were kind gifts from Dr. Péter Várnai (Semmelweis University).

3.9. Transfection of A7R5 cell lines and primary rat VSMCs

A7R5 rat aortic VSMCs (American Type Culture Collection, Rockville, MD, USA) and primary rat VSMC cultures were transfected separately, using differing transfection reagents and protocols to ensure optimal results. These experiments aimed to examine the subcellular localization of CH25H and of various organelle markers. Accordingly, cell cultures were cotransfected with DNA constructs encoding fluorescent fusion proteins. In each case, cells received both the Cerulean-CH25H and one of the mRFP-labeled marker proteins expressing DNA constructs.

A7R5 cells between their third and tenth passages were plated onto μ-Slide 8 well plate (Ibidi) in a 1×10^5 cells/well density and cultured in DMEM containing 10% FBS and 1% penicillin-streptomycin. The next day, A7R5 cells underwent the cotransfection procedure. The three separate DNA construct combinations used were as follows: Cerulean-CH25H + mRFP-SAC1; Cerulean-CH25H + mRFP-TGN38; Cerulean-CH25H + mRFP-Giantin. A7R5 cells were cotransfected with one of the DNA construct combinations using the Lipofectamine 2000 transfection reagent (Invitrogen). Briefly, a total of 0.15 μg plasmid DNA (0.075 μg - 0.075 μg of each DNA construct used) and 0.27 μl Lipofectamine 2000 were diluted respectively in equal amounts (100 μl - 100 μl) of Opti-MEM (Gibco) and incubated at room temperature for 5 minutes. The diluted DNA and Lipofectamine 2000 were then mixed at a 1:1 ratio and incubated at room temperature for 20 minutes before adding the 200 μl mixture to one well. A7R5 cells were kept in a cell culture incubator (5% CO2; 37°C) for 6 hours, then the transfection medium was replaced with DMEM (10% FBS; 1% penicillin-streptomycin) and cells were incubated for further 24 hours.

The primary rat VSMCs were plated onto μ-Slide 8 well plate in a 1×10^5 cells/well density and cultured in supplemented DMEM (10% FBS; 1% penicillin–streptomycin; 1% GlutaMAX). We transfected VSMCs the following day using the FuGENE 6 transfection reagent (Promega). VSMCs were cotransfected with Cerulean-CH25H and mRFP-SAC1 constructs, the total amount of DNA was 0.5 μg DNA/well, meaning 0.25 μg-0.25 μg of each DNA construct. We applied a 3:1 = FuGENE 6:DNA ratio. For the cotransfection of one well we incubated 1.5 μl of FuGENE 6 in 25 μl supplemented DMEM at room temperature for 5 minutes. Then, we added appropriate volumes of each DNA construct (containing 0.25 μg of DNA) and incubated the mixture for 15 more minutes. 25 μl of the FuGENE 6 and DNA mixture was then added to one culture well containing 250 μl of supplemented DMEM. VSMCs were then incubated for 24 hours in a cell culture incubator (5% CO2; 37°C).

3.10. Microscopy

To detect fluorescent signals of the expressed fluorescent fusion proteins in transfected rat primary VSMCs and A7R5 cells as well as the immunolabeled endogeneous smooth muscle alpha-actin in rat primary VSMCs, we utilized confocal laser-scanning microscopy (Zeiss LSM 710). The transfected cells were subjected to imaging 24 hours after transfection, whereas smooth muscle alpha-actin was imaged after the completion of the immunocytochemistry procedure. Obtained images were processed with Fiji 1.53q software [104]. We analyzed the colocalization of Cerulean-CH25H and mRFP fusion protein signals using the JACoP plugin [105]. To define the degree of colocalization we examined Pearson's correlation coefficient values of the analysis.

3.11. Liquid chromatography–tandem mass spectrometry (LC-MS/MS)

LC-MS/MS was performed by Pál Szabó (Research Center for Natural Sciences). The procedure was carried out as described by Pál Szabó in our previous study [103] "A total of 900 μL of methanol was used for 300 μL of supernatant samples for protein precipitation. The supernatants were obtained from 6-well plates, in which the cells were cultured in 1 mL of medium. The samples were vortexed and centrifuged for 5 min at 13,000 rpm. A total of 100 μL of supernatant was pipetted into a micro-vial and used for quantitation. LC-MS/MS measurements were run on a Sciex 6500QTrap mass spectrometer coupled with an Agilent 1100 HPLC system. A Kinetex EVO-C18, 50 × 2.1

mm, 5 µm HPLC column was applied using water and acetonitrile (both containing 0.1% formic acid) in that gradient elution mode. The flow rate was 600 µL/min. The mass spectrometer was operated in positive APCI ionization. The needle current was set to 3 µA. Curtain, evaporating, and drying gasses were 40, 30, and 20 psi, respectively. Quantitation was completed in the MRM mode using ion transitions: 382.5/367.2, 367.2/161.3, 385.2/159, and 367.3/159. The dwell time for each transition was 150 msec."

3.12. Statistical analysis

We used GraphPad Prism 9.1.2 software to perform statistical analysis and to plot graphs. Sample size is indicated in each relevant figure legend as n = number of independent experiments. Data are shown as mean ± SEM. The qRT-PCR and 25-HC concentration data were analyzed using the multiple linear regression procedure with a 95% confidence interval. In the case of the experiments employing inhibitors, the significance of inhibitor treatment, hormone stimuli, and their interaction with the dependent variable was determined. To analyze data displayed in Figure 8B, we applied the unpaired *t*-test, which was suitable for comparison of the control and the stimulated groups.

4. Results

4.1. *Ch25h* gene expression is upregulated in response to AngII stimulus in primary rat VSMCs

As oxysterols and 25-HC play a prominent role in atherogenic processes [77,106] and the skeletal muscle wasting effect of AngII was shown to be mediated by 25-HC [101], we were curious to see whether there is any connection between AngII and 25-HC in a vascular context. To investigate this possibility, we examined whether AngII affected *Ch25h* - encoding CH25H protein - expression in primary rat VSMCs.

We utilized multiple time points to assess the time kinetics of AngII-induced gene expression change. VSMCs were stimulated with 100 nM AngII for 1, 2, 3, 4, 5, or 6 hours, the negative control group received no stimulation. *Ch25h* mRNA levels in the samples were measured using qRT-PCR. Figure 7 shows that *Ch25h* mRNA levels increased in response to the AngII stimulus. The peak of *Ch25h* mRNA levels was observed in the group that was stimulated for 1 hour. Here AngII induced a more than fifty-fold increase compared to the baseline *Ch25h* mRNA levels **(Figure 7)**. Since the 1-hour-long AngII stimulus resulted in the most pronounced upregulation of *Ch25h*, we chose this time point for further analysis.

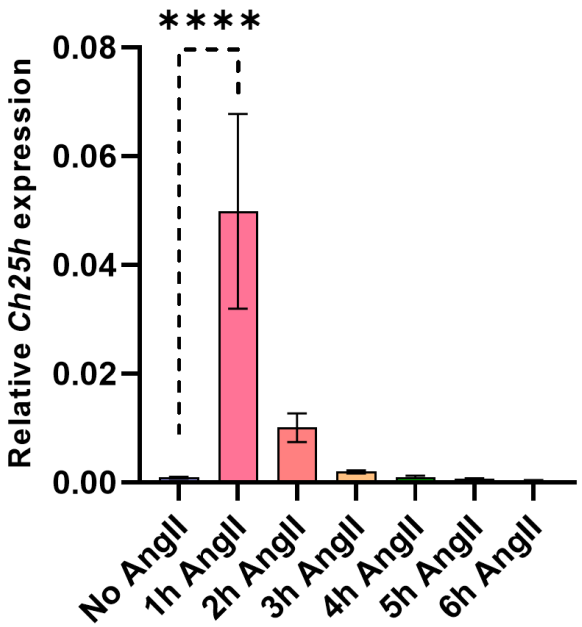

Figure 7. AngII induces the upregulation of *Ch25h* in rat VSMCs. We incubated primary rat VSMCs in serum-free media overnight. Then VSMCs were stimulated with 100 nM AngII for various timespans or not stimulated. Following mRNA isolation and cDNA

preparation, samples were subjected to qRT-PCR measurement to determine *Ch25h* mRNA levels. *Ch25h* mRNA levels are shown relative to *Gapdh* mRNA levels. The figure depicts mean values ± SEM of n = 5 independent experiments. Data were analyzed using multiple linear regression, **** $p < 0.0001$. Source: Kovács KB *et al.* [103].

4.2. AT1R and $G_{q/11}$ activity is responsible for AngII-induced *Ch25h* upregulation in primary rat VSMC

We hypothesized that *Ch25h* upregulation by AngII was achieved through the activity of AT1R. In order to investigate this hypothesis, we employed candesartan, a potent insurmountable antagonist of AT1R, used in antihypertensive therapy [107].

VSMCs were pretreated with 10 μM candesartan for 30 minutes prior to 1 hour of AngII (100 nM) or vehicle stimulus. The control group received DMSO pretreatment before stimuli. In accordance with our expectations, the candesartan pretreatment completely abolished the AngII-induced *Ch25h* upregulation **(Figure 8A)**.

We also investigated signaling molecules downstream of AT1R. As described previously, AT1R activation is able to trigger signaling through both $G_{q/11}$ protein and β-arrestin [14]. To assess the role of the $G_{q/11}$ function in the upregulation of *Ch25h* VSMCs, we utilized YM-254890, a $G_{q/11}$ inhibitor. The YM-254890 was applied at a concentration of 1 μM, the pretreatment lasted for 30 minutes and VSMCs were then stimulated with 100 nM AngII or vehicle for 1 hour. Figure 8A shows that YM-254890 pretreatment rendered AngII unable to induce *Ch25h* upregulation.

β-arrestin-dependent signaling can be activated with the TRV120023 (TRV3) biased AT1R agonist, which selectively activates the β-arrestin but not the $G_{q/11}$ pathway [108–111]. VSMCs were stimulated with 3 μM TRV3 peptide for one hour. The TRV3 stimulus was insufficient to induce *Ch25h* upregulation in VSMCs **(Figure 8B)**.

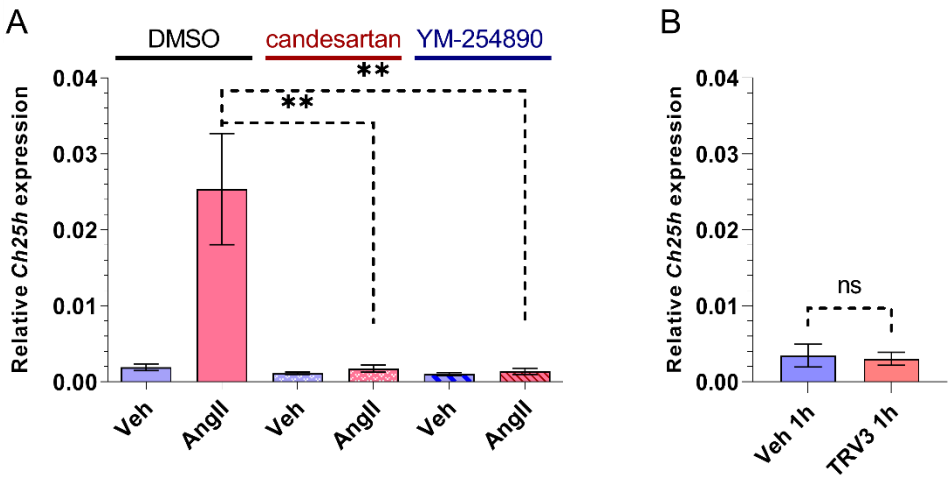

Figure 8. AT1R- and $G_{q/11}$- dependent *Ch25h* gene expression in rat VSMCs in response to AngII. **(A)** VSMCs were serum deprived overnight. The next day, we pretreated VSMCs with 10 µM candesartan or 1 µM YM-254890 for 30 minutes. The control group received DMSO pretreatment. VSMCs were then stimulated with 100 nM AngII or vehicle (Veh) for 1 hour. Following mRNA isolation and cDNA preparation, samples were subjected to qRT-PCR measurement to determine *Ch25h* mRNA levels. *Ch25h* mRNA levels are shown relative to *Gapdh* mRNA levels. The figure depicts mean values ± SEM of n = 4–5 independent experiments. Data were analyzed using multiple linear regression, ** $p < 0.01$. **(B)** VSMCs were serum deprived overnight then stimulated with 3 µM TRV120023 (TRV3) or vehicle (Veh) for 1 hour. Following mRNA isolation and cDNA preparation, samples were subjected to qRT-PCR measurement to determine *Ch25h* mRNA levels. *Ch25h* mRNA levels are shown relative to *Gapdh* mRNA levels. The figure depict mean values ± SEM of n = 3 independent experiments. Data were analyzed using unpaired *t*-test, ns: not significant. Source: Kovács KB *et al.* [103]

4.3. Role of the MAP kinase family proteins in AngII-induced gene expression changes in primary rat VSMCs

Our data showed that inhibition of $G_{q/11}$-protein activity in VSMCs is sufficient to wipe out AngII-induced *Ch25h* upregulation. Based on this information, we investigated the role of MAP kinase family proteins, such as ERK1/2, p38 mitogen-activated protein kinase (p38 MAPK), and c-Jun N-terminal kinase (JNK), which are activated by $G_{q/11}$ actions and are also implicated in *Ch25h* upregulation [8,68,112,113]. The activity of the kinases was blocked using various pharmacological inhibitors such as the mitogen-activated protein kinase kinase (MEK) inhibitor PD98059 (20 µM) for the elimination of ERK1/2 activity, SB202190 (50 µM) for p38 MAPK activity inhibition, and JNK-IN-8 (IN-8; 1 µM) to inhibit JNKs **(Figure 9A-C)**. Inhibitor pretreatment lasted for 30 minutes, the control group received DMSO pretreatment. Following pretreatment, the VSMCs

were stimulated with 100 nM AngII or vehicle for 1 hour. We found that the PD98059 pretreatment resulted in a slightly reduced AngII-induced *Ch25h* upregulation **(Figure 9A)**. The inhibition of JNK activity did not affect the *Ch25h* expression either in the vehicle- or in the AngII-stimulated samples **(Figure 9B)**. However, the SB202190 pretreatment effectively wiped out AngII-induced *Ch25h* upregulation **(Figure 9C)**. The *Ch25h* expression in response to AngII was significantly lower in the SB202190 group compared to the DMSO control. The p38 MAPK inhibition was sufficient to hinder *Ch25h* upregulation in VSMCs.

We also wanted to see how the lack of ERK and p38 MAPK activity affected other AngII-induced gene expression changes. We set out to investigate the expression of dual-specificity MAPK phosphatases (DUSPs). DUSPs are the specific regulators of MAPKs. They catalyze the dephosphorylation of their activation loop. DUSPs are able to bind their substrates even in a dephosphorylated state thus they can exert spatiotemporal regulation of MAPKs [114]. Furthermore, it was demonstrated that the expression of *Dusp* genes was upregulated in response to growth factor and mitogenic stimuli [115]. In accordance, our group identified the upregulation of *Dusp5*, *Dusp6* and *Dusp10* in response to AngII in primary rat VSMCs [37].

To conduct this investigation, we utilized the inhibitors mentioned above. Primary rat VSMCs were pretreated with PD98059 (20 μM), SB202190 (50 μM) or DMSO for 30 minutes, followed by a 2-hour long AngII (100nM) or vehicle stimulus. Similarly to the observation in the case of *Ch25h*, the inhibition of MEK, and thereby ERK, resulted in a reduced AngII-induced expression of *Dusp* isoforms **(Figure 10A-C)**, which was significant in the case of *Dusp6* **(Figure 10B)**. The inhibition of p38 MAPK also resulted in a significant decrease of *Dusp5* and *Dusp6* expression in the groups stimulated with AngII **(Figure 10D-E)**. In contrast, by the *Dusp10* isoform, neither the inhibition of MEK nor the inhibition of p38 MAPK caused a significant decrease of AngII-induced upregulation, when compared to the DMSO pretreated control group **(Figure 10C and 10F)**.

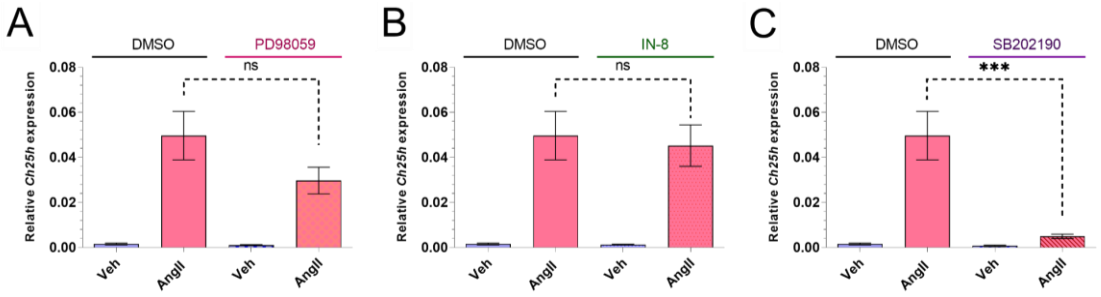

Figure 9. p38 MAPK has a substantial role in AngII-induced *Ch25h* gene expression in rat VSMCs. VSMCs were serum deprived overnight. The next day, we pretreated VSMCs with 20 μM PD98059 **(A)**, 1 μM JNK-IN-8 (IN-8) **(B)**, or 50 μM SB202190 **(C)** for 30 minutes. The control group received DMSO pretreatment. VSMCs were then stimulated with 100 nM AngII or vehicle (Veh) for 1 hour. Following mRNA isolation and cDNA preparation, samples were subjected to qRT-PCR measurement to determine *Ch25h* mRNA levels. *Ch25h* mRNA levels are shown relative to *Gapdh* mRNA levels. The figure depicts mean values ± SEM of n = 6 independent experiments. Data were analyzed using multiple linear regression, *** $p < 0.001$, ns: not significant. Source: Kovács KB *et al.* [103]

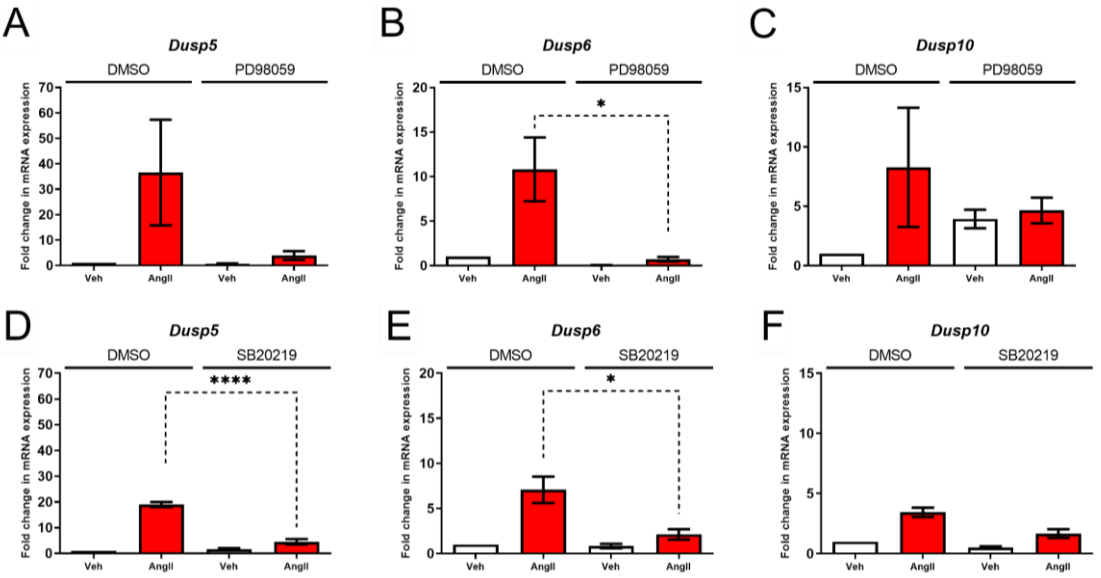

Figure 10. Effect of MAP kinase family inhibitors on the AngII-induced upregulation of *Dusp* isoforms. VSMCs were serum deprived overnight. The next day we pretreated VSMCs with 20 μM PD98059 **(A-C)**, or 50 μM SB202190 **(D-F)** for 30 minutes. The control group received DMSO pretreatment. VSMCs were then stimulated with 100 nM AngII or vehicle (Veh) for 2 hours. Following mRNA isolation and cDNA preparation, samples were subjected to qRT-PCR measurement to assess *Dusp5* **(A and D)**, *Dusp6* **(B and E)** and *Dusp10* **(C and F)** mRNA levels relative to *Gapdh* mRNA levels. The mRNA expression data were normalized to the mRNA levels determined in the DMSO vehicle samples. These fold change values are plotted as the mean ± SEM of n = 3 independent experiments. Data were analyzed using multiple linear regression, **** $p < 0.0001$, * $p < 0.05$. Source: Gém JB *et al.* [37]

4.3.1. Effect of pharmacological inhibitors on the phosphorylation of p38 MAPK and STAT1

We wanted to assess how the inhibitors that were effective in abolishing AngII-induced *Ch25h* upregulation alter the activity of p38 MAPK and the transcription factor STAT1. Prior literature data suggest that STAT1 promotes *Ch25h* expression [74]. We investigated the phosphorylation status of p38 MAPK Thr180/Tyr182 and STAT1 Ser727 residues, which indicates the activity of the respective proteins.

Primary VSMCs were pretreated for 30 minutes with YM-254890 (1 µM) $G_{q/11}$ inhibitor or SB202190 (50 µM) p38 MAPK inhibitor, whereas the control group received DMSO pretreatment. Following pretreatment VSMCs were stimulated with either vehicle or 100 nM AngII. VSMCs were lysed with a 2X Laemmli sample buffer and subjected to Western blot procedure.

Our Western blot data showed that AngII induced the phosphorylation of both p38 MAPK and STAT1 on the amino acid residues investigated **(Figure 11A-D)**. We found that the YM-254890 pretreatment caused the decrease of phosphorylation in both p38 MAPK and STAT1, although the former change was not significant **(Figure 11A and 11C)**. Similarly, the p38 MAPK inhibitor SB202190 reduced the phosphorylation in both the p38 MAPK and STAT1 proteins **(Figure 11B and 11D)**.

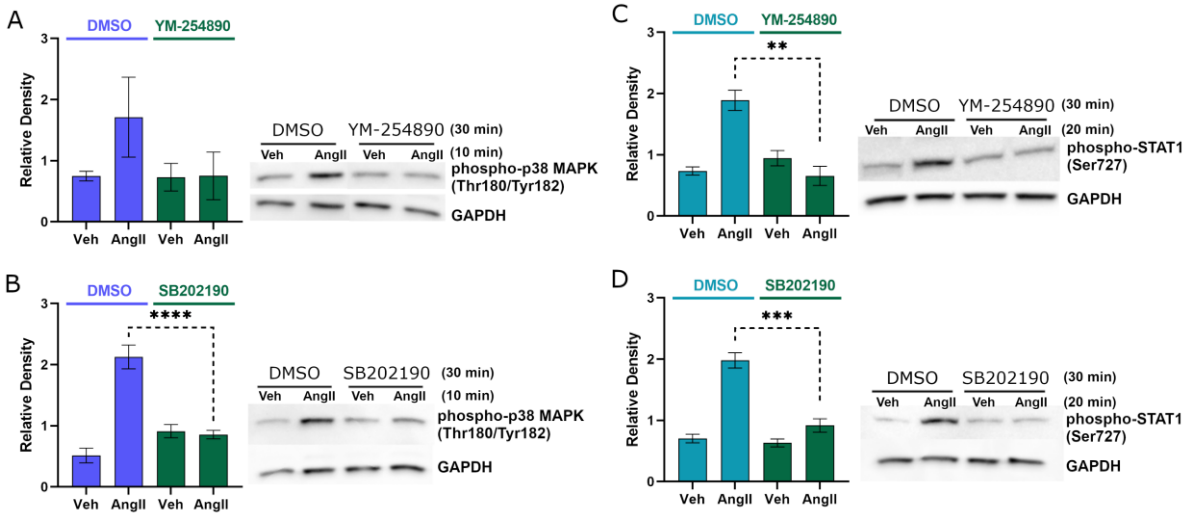

Figure 11. The $G_{q/11}$ and p38 MAPK inhibitors reduce AngII-induced p38 MAPK and STAT1 phosphorylation. Serum-deprived VSMCs were pretreated for 30 minutes with YM-254890 ($G_{q/11}$ inhibitor; 1 µM), SB202190 (p38 MAPK inhibitor; 50 µM) or DMSO as control **(A-D)**. VSMCs were then stimulated with 100 nM AngII or vehicle for 10 minutes **(A-B)** or 20 minutes **(C-D)**. Following lysis with 2X Laemmli buffer, the VSMC samples were subjected to Western blot to detect phospho-p38 MAPK (Thr180/Tyr182)

(A-B) or phospho-STAT1 (Ser727) **(C-D)**. Western blot images were analyzed using Fiji software. The levels of a given phospho-protein are shown relative to the GAPDH level. These relative density values are plotted as the mean ± SEM of n = 3-7 independent experiments. Data were analyzed using multiple linear regression, **** $p < 0.0001$, *** $p < 0.001$, ** $p < 0.01$. Own figure of unpublished data.

4.4. The inhibition of Nox activation does not impact AngII-induced Ch25h upregulation in primary rat VSMCs

We investigated the involvement of Nox activation in AngII-induced *Ch25h* upregulation. We identified two possible ways in which Nox proteins might contribute to the expression of *Ch25h*. Firstly, AngII is known to induce ROS production by activating Nox enzymes [21]. The Nox isoforms whose function is notable in VSMCs are Nox1 and Nox4 [39]. The ROS generation promoted by AngII affects signaling, including the p38 MAPK activation upon AngII stimulus, which was shown to be redox-sensitive [23].

Secondly, oxysterols can be produced by non-enzymatic processes, such as oxidative stress [53] and they are considered endogenous ligands for Liver X Receptors (LXR) [116]. Furthermore, it was found that *Ch25h* upregulation can be the result of LXR activation by 25-HC or LXR agonist T317 [67]. Thus, we hypothesized that Nox activity might affect AngII-induced *Ch25h* upregulation either by influencing p38 MAPK activity or by triggering oxidative stress, which might result in oxysterol production and LXR activation.

We utilized a pharmacological approach and chose the diphenyleneiodonium chloride (DPI) compound to inhibit Nox enzymes in VSMCs. DPI compound potently inhibits a wide range of Nox enzymes, including those expressed in rat VSMCs [40,117–119]. VSMCs were treated with 5 μM of DPI for 30 minutes and subsequently stimulated with 100 nM of AngII for 1 hour. According to the qRT-PCR data, there was no significant difference of *Ch25h* expression between the DMSO- and DPI-treated groups **(Figure 12)**. AngII-induced *Ch25h* upregulation was not affected by the inhibition of Nox enzymes with DPI **(Figure 12)**.

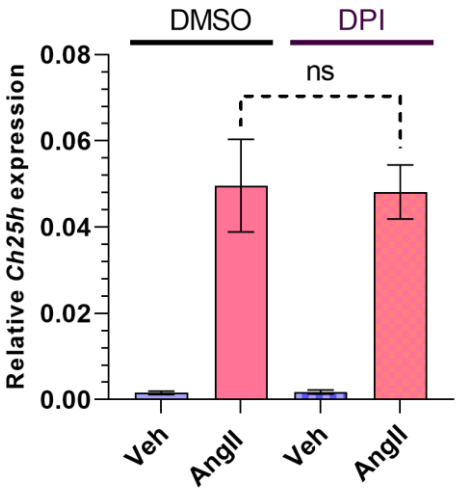

Figure 12. Nox inhibition does not influence *Ch25h* gene expression in rat VSMCs. VSMCs were serum deprived overnight. The next day, we pretreated VSMCs with 5 μM DPI or DMSO for 30 minutes. VSMCs were then stimulated with 100 nM AngII or vehicle (Veh) for 1 hour. Following mRNA isolation and cDNA preparation, samples were subjected to qRT-PCR measurement to determine *Ch25h* mRNA levels. *Ch25h* mRNA levels are shown relative to *Gapdh* mRNA levels. The figure depicts mean values ± SEM of n = 5 independent experiments. Data were analyzed using multiple linear regression, ns: not significant. Source: Kovács KB *et al.* [103]

4.5. CH25H protein localizes to the endoplasmic reticulum in the A7R5 rat VSMC cell line and in primary rat VSMCs

Since CH25H protein has not been investigated in VSMCs before, we aimed to examine its intracellular localization to see how our data compares to the data available in the literature on its localization in other cell types. Previously it was found that both mouse and human CH25H proteins localize to the endoplasmic reticulum (ER) and Golgi compartments in transfected COS, fibroblast-like cells [58]. We utilized a similar approach. Namely, we cotransfected VSMC cultures with DNA constructs expressing either CH25H or various organelle markers and then analyzed the colocalization of their signals.

We designed and created a DNA construct encoding Cerulean-labeled CH25H fusion protein (Cerulean-CH25H). Additionally, we used various mRFP-labeled organelle marker fusion protein encoding DNA constructs: ER marker; phosphatidylinositol-3-phosphatase (SAC1) (mRFP-SAC1), Golgi apparatus membrane marker; (mRFP-Giantin), trans-Golgi network membrane marker (mRFP-TGN38).

A7R5 rat VSMC cell line or primary rat VSMCs were transiently cotransfected with Cerulean-CH25H and one of the marker protein-expressing DNA constructs. 24 hours after transfection, the cells were examined using confocal microscopy. Confocal images were analyzed with the JACoP plugin [105] to assess the colocalization of the two signals.

The fluorescent images and our analysis showed that the Cerulean-CH25H and mRFP-SAC1 proteins presented strong colocalization in the case of A7R5 and primary VSMCs **(Figure 13A)**. However, neither mRFP-Giantin nor mRFP-TGN38 signals showed strong colocalization with the Cerulean-CH25H signal in the transfected A7R5 cells **(Figure 13B)**. Based on our data, the CH25H protein localizes to the ER of VSMCs.

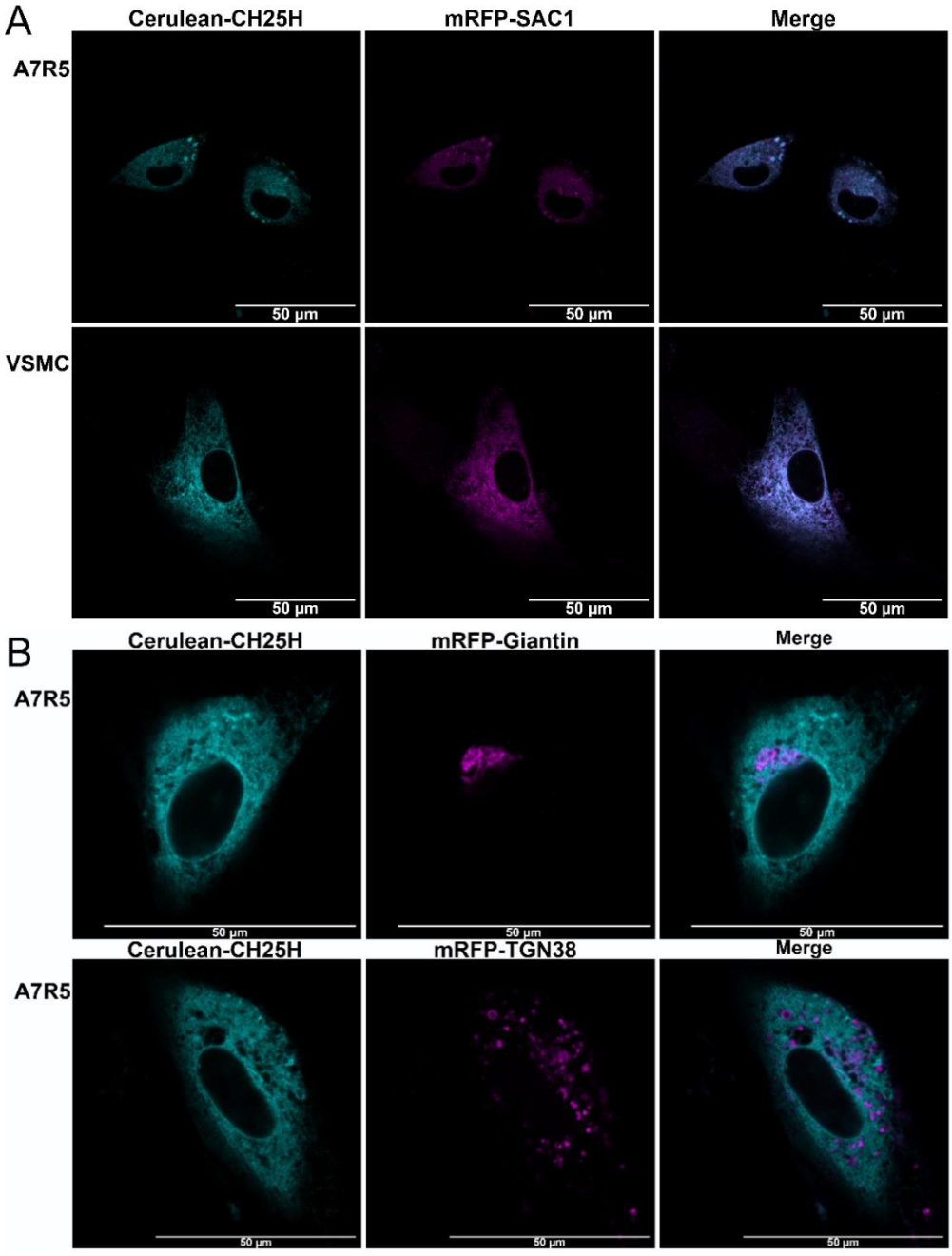

Figure 13. CH25H protein localizes to the ER in VSMCs. A7R5 rat VSMCs (A7R5) and primary rat VSMCs (VSMC) were cotransfected with Cerulean-CH25H (cyan) and mRFP-SAC1 (magenta) expressing DNA constructs **(A)**. In a separate experiment A7R5 cells were cotransfected with either Cerulean-CH25H (cyan) and mRFP-Giantin (magenta) or Cerulean-CH25H (cyan) and mRFP-TGN38 (magenta) fusion protein expressing DNA constructs **(B)**. 24 hours post-transfection we used a confocal microscope (Zeiss LSM710) for imaging and subsequently analyzed colocalization of fluorescent signals using Fiji software. Pearson's correlation coefficient (PCC) values were assessed in each case. In the case of Cerulean-CH25H and mRFP-SAC1 signals PCC = 0.83 ± 0.038 = mean ± SEM in A7R5 cells, and PCC = 0.85 ± 0.01 = mean ± SEM in VSMC, n = 5 independent experiments **(A)**. In the case of Cerulean-CH25H and mRFP-Giantin signals PCC = 0.29±0.014 = mean±SEM, whereas in the case of Cerulean-CH25H and mRFP-TGN38 PCC = 0.41±0.013 = mean±SEM, n = 3 independent experiments **(B)**. Scale bars represent 50 μm. Source: Kovács KB *et al.* [103]

4.6. AngII-stimulated primary rat VSMCs release 25-HC

We wanted to gather information about the product of the CH25H enzyme to see whether the AngII-induced *Ch25h* upregulation also translates to 25-HC level changes. We chose to examine extracellular 25-HC levels in our VSMC cultures since literature data demonstrates that 25-HC can be released by cells. For instance, 25-HC was shown to be secreted by macrophages in a previous study [68]. Furthermore, 25-HC - once released to the extracellular compartment - has the potential to evoke cellular responses via the binding of cell surface proteins [64].

In order to investigate 25-HC levels in the supernatant of VSMCs, long-term AngII stimuli were employed. A concentration of 1 μM AngII was used and stimuli of VSMC cultures lasted for 2, 4, 8, 16, and 24 hours. Following the hormone stimulus, 1 ml of the supernatants was collected. 25-HC levels in the various supernatant samples were assessed with LC-MS/MS. Figure 14 demonstrates the progressive increase of 25-HC concentration up until the 4-hour time point, where an average of 8.2 ng/ml is reached. After the 16-hour time point, 25-HC levels in the VSMC supernatants return to approximately the baseline levels. We found that 25-HC concentrations were significantly increased in the supernatant of the group stimulated with AngII for 4 hours compared to that of the non-stimulated group.

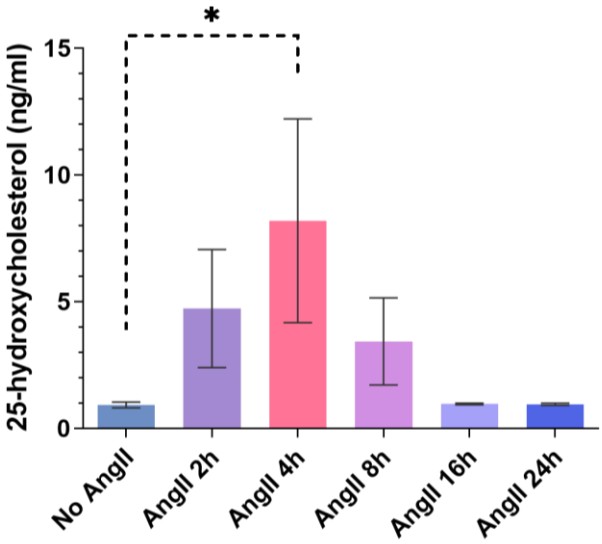

Figure 14. AngII induces 25-HC production by VSMCs. Following serum deprivation, primary rat VSMCs were stimulated with AngII (1 μM) for differing timespans (2, 4, 8, 16, or 24 hours) or not stimulated. We collected supernatants of the VSMCs and assessed 25-HC concentration with LC-MS/MS technique. Average 25-HC concentration values are shown as mean ± SEM based on n = 3 independent experiments. Statistical analysis was carried out using multiple linear regression, * $p < 0.05$. Source: Kovács KB *et al.* [103]

5. Discussion

In this study, we identified *Ch25h* upregulation in VSMCs as a response to AngII stimulus, which is an AT1R and $G_{q/11}$ dependent gene expression change. We determined that p38 MAPK activity is crucial to *Ch25h* upregulation. The CH25H protein localizes to the ER in VSMCs and is active in these cells, as evidenced by the 25-HC concentration data obtained from the supernatant of AngII-stimulated VSMC cultures. The proinflammatory effects of AngII in vascular pathology are similar to those of 25-HC [33,47,69,70,81]. By investigating the underlying connection between 25-HC production and AngII-induced gene expression changes, we aimed to gather a more profound understanding of AngII functions in the vasculature.

We identified for the first time the upregulation of the *Ch25h* gene by AngII in primary rat VSMCs. Our qRT-PCR data showed an approximately fifty-fold increase of *Ch25h* mRNA in the group stimulated with AngII for one hour **(Figure 7)**. Three hours after the AngII stimulus, the *Ch25h* mRNA levels were comparable to the baseline levels detected in the non-stimulated group **(Figure 7)**. These results suggest that AngII-induced upregulation of *Ch25h* is not sustained in VSMCs. In contrast, earlier studies investigating the expression change of *Ch25h* in immune cells report an increase of *Ch25h* expression 4 or 6 hours after the stimulus [66,68,120]. In immune cells, the lipopolysaccharide (LPS) serves as a stimulus for *Ch25h* expression [66]. The finding that *Ch25h* mRNA level increase in VSMCs showed to be quick and transient indicates that its expression is regulated in a different manner than in immune cells. This phenomenon may be attributed to the differing nature of the stimulus inducing the *Ch25h* upregulation or a distinct regulation of the *Ch25h* mRNA levels in VSMCs. A study conducted on an osteoarthritis model found that microRNA targeting of *Ch25h* proves beneficial in the reversal of CH25H-mediated effects [121]. Considering this data, the involvement of microRNAs might explain the transient expression of *Ch25h* in VSMCs.

We utilized a pharmacological approach to determine the signaling pathway leading to *Ch25h* upregulation in VSMCs. We treated VSMCs with candesartan, a potent AT1R antagonist, prior to the AngII stimulus. The candesartan pretreatment blocked AngII-induced *Ch25h* upregulation **(Figure 8A)**. This result demonstrates that AngII upregulates *Ch25h* through the activation of AT1R. Signaling through AT1R causes G protein and β-arrestin dependent actions as well [8,13]. In order to distinguish these

pathways, we stimulated VSMCs with TRV120023, a β-arrestin-biased agonist of AT1R, to see whether it can induce *Ch25h* gene expression change. Our gene expression data showed that TRV120023 was insufficient to induce *Ch25h* expression **(Figure 8B)**. In contrast, the inhibition of $G_{q/11}$ with the YM-254890 substance obliterated AngII-induced *Ch25h* upregulation **(Figure 8A)**. Based on these findings, we conclude that the AngII-induced upregulation of *Ch25h* in VSMCs is dependent on AT1R and $G_{q/11}$ activation.

To further illuminate the actors in the relevant signaling, we investigated signaling proteins downstream of $G_{q/11}$ whose role in *Ch25h* expression was also documented in the literature. AngII-induced effects and $G_{q/11}$ functions contribute to the activation of ERK1/2, p38 MAPK, and JNK [8,112,113]. Additionally, the TLR4-mediated *Ch25h* upregulation in macrophages was shown to be dependent on p38 MAPK and JNK [68]. Our results demonstrated that the inhibition of p38 MAPK with SB202190 but not the inhibition of JNK with JNK-IN-8 wiped out AngII-induced *Ch25h* expression in VSMCs **(Figure 9B-C)**. This indicates the substantial role of p38 MAPK in AngII-induced *Ch25h* upregulation. Furthermore, this result shows that JNK has no effect on *Ch25h* expression in VSMCs, which is in contrast to signaling events documented in macrophages [68].

To investigate the role of ERK1/2 in *Ch25h* upregulation, we utilized the PD98059 MEK inhibitor. qRT-PCR data showed that the PD98059 pretreatment slightly reduced the AngII-induced *Ch25h* expression, but this decrease of *Ch25h* mRNA was not significant compared to the DMSO-treated control group **(Figure 9A)**. This suggests that the role of MEK and ERK1/2 is not essential in AngII-induced *Ch25h* upregulation.

Similarly to *Ch25h*, AngII also induced the upregulation of various *Dusp* isoforms [37]. To see whether these induced gene expression events are the result of the same signaling events as in the case of *Ch25h*, we investigated the involvement of p38 MAPK and ERK1/2 - whose inhibition affected AngII-induced *Ch25h* expression - in the upregulation of *Dusp5*, *Dusp6*, and *Dusp10*. p38 MAPK inhibition significantly reduced *Dusp5* and *Dusp6* expression, but had a less pronounced effect on *Dusp10* expression **(Figure 10D-F)**. Indirect inhibition of ERK1/2 activity attenuated *Dusp5* and *Dusp10* expression, whereas *Dusp6* expression was significantly decreased in the PD98059-treated group compared to the DMSO-treated group **(Figure 10A-C)**. These results indicate that p38 MAPK and ERK1/2 activation affects both *Ch25h* and *Dusp* upregulation in VSMCs. However, in the case of *Dusp*s it seems that the expression of

the various isoforms is differently affected by the p38 MAPK and ERK1/2. This difference might be explained by the fact that MAPK family proteins tend to promote the expression of those phosphatases that specifically regulate them. In this way, the role of p38 MAPK and ERK1/2 in AngII-induced *Dusp* upregulation can be understood as a temporal negative feedback regulatory process [115].

The upregulation of *Ch25h* by the p38 MAPK signaling in VSMCs might rely on mechanisms different from the upregulation of *Dusp*s. This is suggested by the differing time kinetics of the mRNA level changes observed in *Ch25h* and *Dusp*s. The *Ch25h* mRNA levels peak at 1 hour post-stimulus **(Figure 7)**, whereas *Dusp* mRNA levels are at a peak 2 hours post-stimulus [37] **(Figure 10A-F)**. However, if we look at existing literature data, we may understand events downstream of p38 MAPK that lead to *Ch25h* upregulation. The substrates of p38 MAPK include transcription factors, such as STAT1, which is phosphorylated on the 727 Serine (Ser727) residue by p38 MAPK [122]. *Ch25h* is an interferon-stimulated gene and its expression is induced by both interferon (IFN) α and IFNγ. Additionally STAT1 transcription factor promotes the *Ch25h* expression in macrophages [71,74]. In order to see whether the p38 MAPK phosphorylates STAT1 in our samples, we examined the phosphorylation status of STAT1 on Ser727 in AngII-stimulated VSMCs using Western blot. Our results showed that phosphorylation of Ser727 is promoted by AngII stimulus **(Figure 11C-D)**. However, the inhibition of both $G_{q/11}$ with YM-254890 **(Figure 11C)** and p38 MAPK with SB202190 **(Figure 11D)** reduced AngII-induced Ser727 phosphorylation in STAT1. These results are not surprising since both inhibitors reduced AngII-induced p38 MAPK phosphorylation on the Thr180/Tyr182 residues as well **(Figure 11A-B)**. Taken together, we showed that STAT1 phosphorylation in our AngII-stimulated VSMC samples depends on p38 MAPK activity **(Figure 11C-D)**.

Based on the results of these experiments and the above discussed qRT-PCR data, we hypothesize that AngII-induced $G_{q/11}$ signaling activates the p38 MAPK, which then activates STAT1 and ultimately enables *Ch25h* expression in VSMCs. This model is in agreement with the literature data. However, further investigations are needed to confirm the role of STAT1 in AngII-induced *Ch25h* upregulation in VSMCs.

We explored whether oxidative stress influences *Ch25h* expression in VSMCs. AngII promotes ROS production, which alters signaling mechanisms [21,23]. Additionally,

ROS might contribute to oxysterol production and oxysterols have the potential to activate LXR, thus promoting *Ch25h* expression [53,67]. In order to investigate this avenue, we targeted Nox proteins. VSMCs were pretreated with DPI to inhibit Nox activity. We found that the inhibition of Nox enzymes had no effect on AngII-induced *Ch25h* upregulation. Thus our finding indicates that Nox proteins are not involved in this gene expression event in VSMCs **(Figure 12)**.

To assess the subcellular localization of CH25H protein, we cotransfected primary VSMC or A7R5 rat VSMC cultures with DNA constructs encoding Cerulean-labeled CH25H and mRFP-labeled ER or Golgi marker expressing DNA constructs. Our results showed that the Cerulean-CH25H colocalized with the ER marker mRFP-SAC1 **(Figure 13A)**. This result was consistent in both primary VSMCs and A7R5 cells. However, we did not observe a meaningful colocalization of Cerulean-CH25H and mRFP-Giantin or mRFP-TGN38 signals, which both localize to the Golgi compartment **(Figure 13B)**. Taken together these findings, we conclude that the CH25H protein primarily localizes to the ER in the VSMCs, which is in line with existing literature data on the subcellular localization of CH25H [58].

We investigated the effects of AngII on 25-HC levels because 25-HC is primarily produced by the CH25H enzyme, and this approach could provide us with information about the presence and functionality of CH25H in VSMCs [55]. Since 25-HC was shown to be secreted by macrophages, we chose to assess 25-HC levels in the supernatants of VSMC cultures stimulated with AngII for various timespans [68]. Our data showed that VSMCs indeed release 25-HC into their media **(Figure 14)**. The 25-HC concentration in the supernatants of VSMCs was at a peak 4 hours after the AngII stimulus, reaching an average of 8.2 ng/ml. Intriguingly, this 25-HC concentration is comparable to the amount of 25-HC produced by LPS-stimulated immune cells. Izumi *et al.*, using a similar approach to ours, investigated 25-HC concentrations in the supernatants of microglia cultures. According to their results, LPS-induced 25-HC concentration increase was in the ng/ml range, with an average value under 6 ng/ml [123]. Similarly, it was found that LPS stimulus resulted in elevated 25-HC levels in the media of peritoneal macrophage cells, with mean maximal 25-HC concentration ranging between 15 ng/ml and 20 ng/ml [79]. Considering these pieces of literature data, AngII-stimulated VSMCs seem to be able to produce 25-HC to a similar extent as LPS-stimulated immune cells. As for the

change of 25-HC concentration over time, we observed a decrease 8 hours post-stimulus **(Figure 14)**. 16 hours after the AngII stimulus, 25-HC levels were comparable to those of non-stimulated VSMCs **(Figure 14)**. This trend was consistent in all of our experiments.

Thus, we conclude that AngII induces the production of 25-HC, which shows that the CH25H enzyme is active in VSMCs. Notably, 25-HC concentrations in the supernatants of VSMC cultures varied in the ng/ml range. Whereas studies investigating the effects of 25-HC apply 25-HC concentrations of 5 µg/ml - 50 µg/ml, which means a thousand-fold higher concentration range compared to our measurements [64,79,88–91]. However, the dimension of 25-HC concentrations measured in our study can be explained by our experimental design. We assessed 25-HC concentrations in 1 ml of VSMC supernatant. Under these conditions, the 25-HC produced by the VSMC was diluted. The 25-HC released by VSMCs can still be biologically significant, considering that in the interstitium of the vessel wall the dilution would not be as great as in our experimental model. Thus, 25-HC might be an efficient autocrine or paracrine mediator once released by VSMCs. There is evidence that 25-HC binds α5β1 and αvβ3 integrins on the surface of macrophages [64]. The integrin α5β1 is also found in VSMCs where it mediates repair mechanisms during vascular injury and VSMC migration [124,125]. Taken together these findings 25-HC has the potential to mediate signaling through the activation of integrin-related pathways, which is noteworthy for further study.

6. Conclusions

The aims of this study were the identification of the underlying signaling mechanisms that lead to *Ch25h* expression in VSMCs and the investigation of CH25H subcellular localization and action. The major conclusions of this thesis, as per respective objectives, are the following **(Figure 15)**:

6.1. Investigation of AngII-induced *Ch25h* expression in VSMCs and underlying signaling pathways:

→AngII induces the upregulation of *Ch25h* in primary rat VSMCs.

→AngII-induced *Ch25h* upregulation is dependent on AT1R and $G_{q/11}$ activity.

→The p38 MAPK is essential for the AngII-induced *Ch25h* upregulation, whereas ERK1/2 activity has no significant effect on the expression of *Ch25h*.

→The AngII-induced upregulation of *Dusp* isoforms is affected by p38 MAPK and ERK1/2. p38 MAPK is significant in the AngII-induced expression of *Dusp5* and *Dusp6*, whereas ERK1/2 plays a significant role in *Dusp6* expression.

→AngII stimulus of VSMCs causes phosphorylation of p38 MAPK and STAT1 transcription factor. The p38 MAPK activity is necessary for STAT1 phosphorylation on the Ser727 residue.

→Nox functions have no effect on AngII-induced *Ch25h* upregulation in VSMCs.

6.2. Examination of CH25H activity in VSMCs:

→The CH25H enzyme localizes to the ER in VSMC cell lines.

→AngII promotes the production of 25-HC by VSMCs, demonstrating the catalytic activity of the upregulated CH25H in VSMCs.

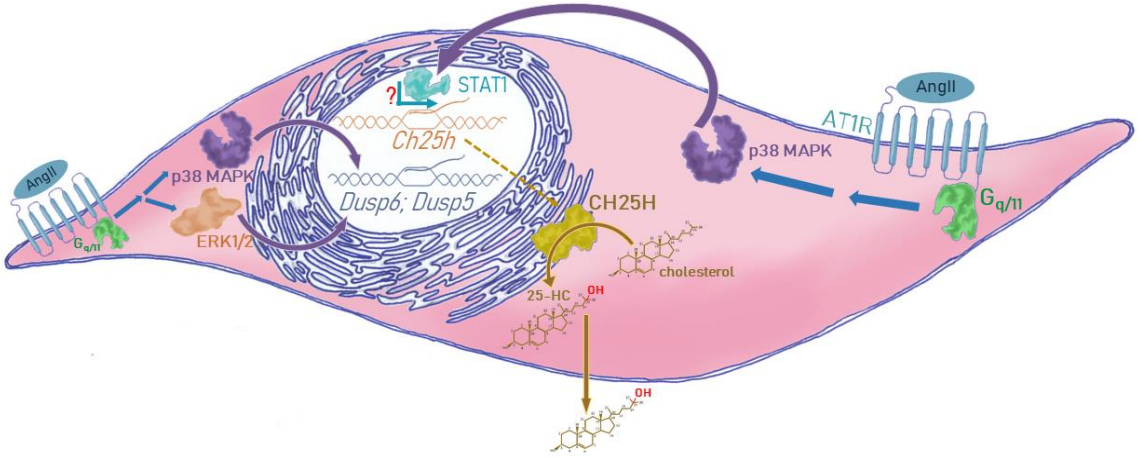

Figure 15. Scheme of AngII-induced signaling that leads to *Dusp* and *Ch25h* expression and 25-HC release. (Own figure based on the conclusions of chapter 6.)

7. Summary

CVD presents major health problems globally. Both the vasoactive hormone AngII and the oxysterol 25-HC contribute to the development of vascular pathologies, thus CVD. In this PhD work, we investigated the relationship between CH25H, the enzyme responsible for 25-HC production, and AngII. We aimed to uncover the AngII-induced gene expression changes and the signaling pathways that lead to them.

The major finding of this thesis is the demonstration of AngII-induced *Ch25h* upregulation in primary rat VSMCs. We determined that *Ch25h* upregulation depends on AT1R and $G_{q/11}$ activation. We examined the role of MAPKs. ERK1/2 inactivity somewhat reduced AngII-induced *Ch25h* upregulation. Instead, we found p38 MAPK to be the crucial kinase that enables *Ch25h* upregulation upon the AngII stimulus. Furthermore, we found that p38 MAPK activity is necessary for the AngII-induced phosphorylation of STAT1 transcription factor, which might be the transcription factor responsible for *Ch25h* upregulation. We further examined whether the ERK1/2 and p38 MAPK mediate AngII-induced *Dusp* upregulation to assess their role in AngII-induced gene expression changes other than *Ch25h*. We showed that p38 MAPK is necessary for both *Dusp5* and *Dusp6* upregulation. However, ERK1/2 is significant only in *Dusp6* upregulation. In contrast, *Dusp10* expression was not significantly influenced either by p38 MAPK or ERK1/2 inhibition. In addition to signaling pathways, we examined the CH25H protein and its product. Using fluorescently labeled fusion proteins, we determined that CH25H localizes to the ER in VSMCs. Importantly, we identified the increase of 25-HC concentration in the supernatant of AngII-stimulated VSMCs, indicating the functionality of CH25H in this cell type.

In this study, we established that AngII upregulates *Ch25h* expression and that VSMCs can be a source of 25-HC production, which was previously not documented in the literature. We found that the activation of growth-related signaling by AT1R is needed for the AngII-induced *Ch25h* upregulation. We demonstrated that p38 MAPK orchestrates not only the AngII-induced *Ch25h* upregulation but the upregulation of other genes affected by the hormone, namely *Dusp5* and *Dusp6* [37,103]. Furthermore, we showed that AngII stimulus causes 25-HC level elevation in VSMC cultures, which is notable since 25-HC has the potential to act as an autocrine or paracrine mediator in the vessel wall.

8. References

[1] Patel S, Rauf A, Khan H, Abu-Izneid T. Renin-angiotensin-aldosterone (RAAS): The ubiquitous system for homeostasis and pathologies. Biomed Pharmacother 2017;94:317–25. https://doi.org/10.1016/j.biopha.2017.07.091.

[2] Kurtz A. Control of Renin Synthesis and Secretion. Am J Hypertens 2012;25:839–47. https://doi.org/10.1038/ajh.2011.246.

[3] Abdel Ghafar MT. An overview of the classical and tissue-derived renin-angiotensin-aldosterone system and its genetic polymorphisms in essential hypertension. Steroids 2020;163:108701. https://doi.org/10.1016/j.steroids.2020.108701.

[4] Danser AH, van Kats JP, Admiraal PJ, Derkx FH, Lamers JM, Verdouw PD, Saxena PR, Schalekamp MA. Cardiac renin and angiotensins. Uptake from plasma versus in situ synthesis. Hypertension 1994;24:37–48. https://doi.org/10.1161/01.HYP.24.1.37.

[5] Peters J. Cytosolic (pro)renin and the matter of intracellular renin actions. Front Biosci-Sch 2013;5:198–205. https://doi.org/10.2741/S366.

[6] De Mello WC, Frohlich ED. On the local cardiac renin angiotensin system. Basic and clinical implications. Peptides 2011;32:1774–9. https://doi.org/10.1016/j.peptides.2011.06.018.

[7] Kobori H, Nangaku M, Navar LG, Nishiyama A. The Intrarenal Renin-Angiotensin System: From Physiology to the Pathobiology of Hypertension and Kidney Disease. Pharmacol Rev 2007;59:251–87. https://doi.org/10.1124/pr.59.3.3.

[8] Forrester SJ, Booz GW, Sigmund CD, Coffman TM, Kawai T, Rizzo V, Scalia R, Eguchi S. Angiotensin II Signal Transduction: An Update on Mechanisms of Physiology and Pathophysiology. Physiol Rev 2018;98:1627–738. https://doi.org/10.1152/physrev.00038.2017.

[9] Touyz RM, Alves-Lopes R, Rios FJ, Camargo LL, Anagnostopoulou A, Arner A, Montezano AC. Vascular smooth muscle contraction in hypertension. Cardiovasc Res 2018;114:529–39. https://doi.org/10.1093/cvr/cvy023.

[10] Oppermann M, Freedman NJ, Alexander RW, Lefkowitz RJ. Phosphorylation of the Type 1A Angiotensin II Receptor by G Protein-coupled Receptor Kinases and Protein Kinase C*. J Biol Chem 1996;271:13266–72.

https://doi.org/10.1074/jbc.271.22.13266.

[11] Balmforth AJ, Shepherd FH, Warburton P, Ball SG. Evidence of an important and direct role for protein kinase C in agonist-induced phosphorylation leading to desensitization of the angiotensin AT1A receptor. Br J Pharmacol 1997;122:1469–77. https://doi.org/10.1038/sj.bjp.0701522.

[12] Qian H, Pipolo L, Thomas WG. Identification of protein kinase C phosphorylation sites in the angiotensin II (AT1A) receptor. Biochem J 1999;343:637–44. https://doi.org/10.1042/bj3430637.

[13] Ahn S, Nelson CD, Garrison TR, Miller WE, Lefkowitz RJ. Desensitization, internalization, and signaling functions of β-arrestins demonstrated by RNA interference. Proc Natl Acad Sci U S A 2003;100:1740–4. https://doi.org/10.1073/pnas.262789099.

[14] Mathieu NM, Nakagawa P, Grobe JL, Sigmund CD. Insights Into the Role of Angiotensin-II AT1 Receptor-Dependent β-Arrestin Signaling in Cardiovascular Disease. Hypertension 2023;81:6–16. https://doi.org/10.1161/HYPERTENSIONAHA.123.19419.

[15] Du J, Sperling LS, Marrero MB, Phillips L, Delafontaine P. G-protein and tyrosine kinase receptor cross-talk in rat aortic smooth muscle cells: thrombin- and angiotensin II-induced tyrosine phosphorylation of insulin receptor substrate-1 and insulin-like growth factor 1 receptor. Biochem Biophys Res Commun 1996;218:934–9. https://doi.org/10.1006/bbrc.1996.0165.

[16] Bouallegue A, Vardatsikos G, Srivastava AK. Role of insulin-like growth factor 1 receptor and c-Src in endothelin-1- and angiotensin II-induced PKB phosphorylation, and hypertrophic and proliferative responses in vascular smooth muscle cellsThis article is one of a selection of papers published in a special issue on Advances in Cardiovascular Research. Can J Physiol Pharmacol 2009;87:1009–18. https://doi.org/10.1139/Y09-056.

[17] Eguchi S, Numaguchi K, Iwasaki H, Matsumoto T, Yamakawa T, Utsunomiya H, Motley ED, Kawakatsu H, Owada KM, Hirata Y, Marumo F, Inagami T. Calcium-dependent epidermal growth factor receptor transactivation mediates the angiotensin II-induced mitogen-activated protein kinase activation in vascular smooth muscle cells. J Biol Chem 1998;273:8890–6.

https://doi.org/10.1074/jbc.273.15.8890.

[18] Eguchi S, Iwasaki H, Inagami T, Numaguchi K, Yamakawa T, Motley ED, Owada KM, Marumo F, Hirata Y. Involvement of PYK2 in angiotensin II signaling of vascular smooth muscle cells. Hypertension 1999;33:201–6. https://doi.org/10.1161/01.hyp.33.1.201.

[19] Eguchi S, Dempsey PJ, Frank GD, Motley ED, Inagami T. Activation of MAPKs by angiotensin II in vascular smooth muscle cells. Metalloprotease-dependent EGF receptor activation is required for activation of ERK and p38 MAPK but not for JNK. J Biol Chem 2001;276:7957–62. https://doi.org/10.1074/jbc.M008570200.

[20] Ohtsu H, Dempsey PJ, Frank GD, Brailoiu E, Higuchi S, Suzuki H, Nakashima H, Eguchi K, Eguchi S. ADAM17 Mediates Epidermal Growth Factor Receptor Transactivation and Vascular Smooth Muscle Cell Hypertrophy Induced by Angiotensin II. Arterioscler Thromb Vasc Biol 2006;26:e133–7. https://doi.org/10.1161/01.ATV.0000236203.90331.d0.

[21] Griendling KK, Minieri CA, Ollerenshaw JD, Alexander RW. Angiotensin II stimulates NADH and NADPH oxidase activity in cultured vascular smooth muscle cells. Circ Res 1994;74:1141–8. https://doi.org/10.1161/01.res.74.6.1141.

[22] Seshiah PN, Weber DS, Rocic P, Valppu L, Taniyama Y, Griendling KK. Angiotensin II Stimulation of NAD(P)H Oxidase Activity. Circ Res 2002;91:406–13. https://doi.org/10.1161/01.RES.0000033523.08033.16.

[23] Ushio-Fukai M, Alexander RW, Akers M, Griendling KK. p38 Mitogen-activated protein kinase is a critical component of the redox-sensitive signaling pathways activated by angiotensin II. Role in vascular smooth muscle cell hypertrophy. J Biol Chem 1998;273:15022–9. https://doi.org/10.1074/jbc.273.24.15022.

[24] Linseman DA, Benjamin CW, Jones DA. Convergence of angiotensin II and platelet-derived growth factor receptor signaling cascades in vascular smooth muscle cells. J Biol Chem 1995;270:12563–8. https://doi.org/10.1074/jbc.270.21.12563.

[25] Heeneman S, Haendeler J, Saito Y, Ishida M, Berk BC. Angiotensin II induces transactivation of two different populations of the platelet-derived growth factor beta receptor. Key role for the p66 adaptor protein Shc. J Biol Chem 2000;275:15926–32. https://doi.org/10.1074/jbc.M909616199.

[26] Taubman MB, Berk BC, Izumo S, Tsuda T, Alexander RW, Nadal-Ginard B. Angiotensin II Induces c-fos mRNA in Aortic Smooth Muscle: Role of Ca2+ mobilization and protein kinase C activation. J Biol Chem 1989;264:526–30. https://doi.org/10.1016/S0021-9258(17)31290-5.

[27] Naftilan AJ, Gilliland GK, Eldridge CS, Kraft AS. Induction of the proto-oncogene c-jun by angiotensin II. Mol Cell Biol 1990;10:5536–40.

[28] Naftilan AJ, Pratt RE, Dzau VJ. Induction of platelet-derived growth factor A-chain and c-myc gene expressions by angiotensin II in cultured rat vascular smooth muscle cells. J Clin Invest 1989;83:1419–24. https://doi.org/10.1172/JCI114032.

[29] Marrero MB, Schieffer B, Paxton WG, Heerdt L, Berk BC, Delafontaine P, Bernstein KE. Direct stimulation of Jak/STAT pathway by the angiotensin II AT1 receptor. Nature 1995;375:247–50. https://doi.org/10.1038/375247a0.

[30] Marrero MB, Schieffer B, Li B, Sun J, Harp JB, Ling BN. Role of Janus Kinase/Signal Transducer and Activator of Transcription and Mitogen-activated Protein Kinase Cascades in Angiotensin II- and Platelet-derived Growth Factor-induced Vascular Smooth Muscle Cell Proliferation*. J Biol Chem 1997;272:24684–90. https://doi.org/10.1074/jbc.272.39.24684.

[31] Kirchmer MN, Franco A, Albasanz-Puig A, Murray J, Yagi M, Gao L, Dong ZM, Wijelath ES. Modulation of vascular smooth muscle cell phenotype by STAT-1 and STAT-3. Atherosclerosis 2014;234:169–75. https://doi.org/10.1016/j.atherosclerosis.2014.02.029.

[32] Bruder-Nascimento T, Chinnasamy P, Riascos-Bernal D, Cau S, Callera G, Touyz R, Tostes R, Sibinga N. Angiotensin II induces Fat1 expression/activation and vascular smooth muscle cell migration via Nox1-dependent reactive oxygen species generation. J Mol Cell Cardiol 2014;66:18–26. https://doi.org/10.1016/j.yjmcc.2013.10.013.

[33] Capers Q, Alexander RW, Lou P, Hector De Leon , Wilcox JN, Ishizaka N, Howard AB, Taylor WR. Monocyte Chemoattractant Protein-1 Expression in Aortic Tissues of Hypertensive Rats. Hypertension 1997;30:1397–402. https://doi.org/10.1161/01.HYP.30.6.1397.

[34] Qi D, Wei M, Jiao S, Song Y, Wang X, Xie G, Taranto J, Liu Y, Duan Y, Yu B, Li H, Shah YM, Xu Q, Du J, Gonzalez FJ, Qu A. Hypoxia inducible factor 1α in

vascular smooth muscle cells promotes angiotensin II-induced vascular remodeling via activation of CCL7-mediated macrophage recruitment. Cell Death Dis 2019;10:544. https://doi.org/10.1038/s41419-019-1757-0.

[35] Jiang B, Xu S, Hou X, Pimentel DR, Cohen RA. Angiotensin II Differentially Regulates Interleukin-1-β-inducible NO Synthase (iNOS) and Vascular Cell Adhesion Molecule-1 (VCAM-1) Expression: ROLE OF p38 MAPK*. J Biol Chem 2004;279:20363–8. https://doi.org/10.1074/jbc.M314172200.

[36] Xu S, Zhi H, Hou X, Jiang B. Angiotensin II modulates interleukin-1β-induced inflammatory gene expression in vascular smooth muscle cells via interfering with ERK-NF-κB crosstalk. Biochem Biophys Res Commun 2011;410:543–8. https://doi.org/10.1016/j.bbrc.2011.06.021.

[37] Gém JB, Kovács KB, Szalai L, Szakadáti G, Porkoláb E, Szalai B, Turu G, Tóth AD, Szekeres M, Hunyady L, Balla A. Characterization of Type 1 Angiotensin II Receptor Activation Induced Dual-Specificity MAPK Phosphatase Gene Expression Changes in Rat Vascular Smooth Muscle Cells. Cells 2021;10:3538. https://doi.org/10.3390/cells10123538.

[38] Touyz RM, Schiffrin EL. Increased generation of superoxide by angiotensin II in smooth muscle cells from resistance arteries of hypertensive patients: role of phospholipase D-dependent NAD(P)H oxidase-sensitive pathways. J Hypertens 2001;19:1245.

[39] Touyz R m., Yao G, Schiffrin E l. c-Src Induces Phosphorylation and Translocation of p47phox. Arterioscler Thromb Vasc Biol 2003;23:981–7. https://doi.org/10.1161/01.ATV.0000069236.27911.68.

[40] Dikalov SI, Dikalova AE, Bikineyeva AT, Schmidt HHHW, Harrison DG, Griendling KK. Distinct Roles of Nox1 and Nox4 in Basal and Angiotensin II-Stimulated Superoxide and Hydrogen Peroxide Production. Free Radic Biol Med 2008;45:1340–51. https://doi.org/10.1016/j.freeradbiomed.2008.08.013.

[41] Laurent S, Boutouyrie P. The Structural Factor of Hypertension. Circ Res 2015;116:1007–21. https://doi.org/10.1161/CIRCRESAHA.116.303596.

[42] Cai Z, Gong Z, Li Z, Li L, Kong W. Vascular Extracellular Matrix Remodeling and Hypertension. Antioxid Redox Signal 2021;34:765–83. https://doi.org/10.1089/ars.2020.8110.

[43] Rao GN, Berk BC. Active oxygen species stimulate vascular smooth muscle cell growth and proto-oncogene expression. Circ Res 1992;70:593–9. https://doi.org/10.1161/01.RES.70.3.593.

[44] Griendling KK, Sorescu D, Lassègue B, Ushio-Fukai M. Modulation of Protein Kinase Activity and Gene Expression by Reactive Oxygen Species and Their Role in Vascular Physiology and Pathophysiology. Arterioscler Thromb Vasc Biol 2000;20:2175–83. https://doi.org/10.1161/01.ATV.20.10.2175.

[45] Peng K, Tian X, Qian Y, Skibba M, Zou C, Liu Z, Wang J, Xu Z, Li X, Liang G. Novel EGFR inhibitors attenuate cardiac hypertrophy induced by angiotensin II. J Cell Mol Med 2016;20:482–94. https://doi.org/10.1111/jcmm.12763.

[46] Libby P, Buring JE, Badimon L, Hansson GK, Deanfield J, Bittencourt MS, Tokgözoğlu L, Lewis EF. Atherosclerosis. Nat Rev Dis Primer 2019;5:1–18. https://doi.org/10.1038/s41572-019-0106-z.

[47] Poznyak AV, Bharadwaj D, Prasad G, Grechko AV, Sazonova MA, Orekhov AN. Renin-Angiotensin System in Pathogenesis of Atherosclerosis and Treatment of CVD. Int J Mol Sci 2021;22:6702. https://doi.org/10.3390/ijms22136702.

[48] Kalra Dinesh, Sivasubramanian Natarajan, Mann Douglas L. Angiotensin II Induces Tumor Necrosis Factor Biosynthesis in the Adult Mammalian Heart Through a Protein Kinase C–Dependent Pathway. Circulation 2002;105:2198–205. https://doi.org/10.1161/01.CIR.0000015603.84788.47.

[49] Ford Carol M., Li Shaohua, Pickering J. Geoffrey. Angiotensin II Stimulates Collagen Synthesis in Human Vascular Smooth Muscle Cells. Arterioscler Thromb Vasc Biol 1999;19:1843–51. https://doi.org/10.1161/01.ATV.19.8.1843.

[50] Kato H, Suzuki H, Tajima S, Ogata Y, Tominaga T, Sato A, Saruta T. Angiotensin II stimulates collagen synthesis in cultured vascular smooth muscle cells. J Hypertens 1991;9:17–22.

[51] Oh GC, Cho H-J. Blood pressure and heart failure. Clin Hypertens 2020;26:1. https://doi.org/10.1186/s40885-019-0132-x.

[52] Montezano AC, Nguyen Dinh Cat A, Rios FJ, Touyz RM. Angiotensin II and Vascular Injury. Curr Hypertens Rep 2014;16:431. https://doi.org/10.1007/s11906-014-0431-2.

[53] Pannu PS, Allahverdian S, Francis GA. Oxysterol generation and liver X receptor-

dependent reverse cholesterol transport: Not all roads lead to Rome. Mol Cell Endocrinol 2013;368:99–107. https://doi.org/10.1016/j.mce.2012.07.013.

[54] Samadi A, Sabuncuoglu S, Samadi M, Isikhan SY, Chirumbolo S, Peana M, Lay I, Yalcinkaya A, Bjørklund G. A Comprehensive Review on Oxysterols and Related Diseases. Curr Med Chem 2021;28:110–36. https://doi.org/10.2174/0929867327666200316142659.

[55] Diczfalusy U. On the formation and possible biological role of 25-hydroxycholesterol. Biochimie 2013;95:455–60. https://doi.org/10.1016/j.biochi.2012.06.016.

[56] Mutemberezi V, Guillemot-Legris O, Muccioli GG. Oxysterols: From cholesterol metabolites to key mediators. Prog Lipid Res 2016;64:152–69. https://doi.org/10.1016/j.plipres.2016.09.002.

[57] Kandutsch AA, Chen HW. Inhibition of Sterol Synthesis in Cultured Mouse Cells by Cholesterol Derivatives Oxygenated in the Side Chain. J Biol Chem 1974;249:6057–61. https://doi.org/10.1016/S0021-9258(19)42218-7.

[58] Lund EG, Kerr TA, Sakai J, Li WP, Russell DW. cDNA cloning of mouse and human cholesterol 25-hydroxylases, polytopic membrane proteins that synthesize a potent oxysterol regulator of lipid metabolism. J Biol Chem 1998;273:34316–27. https://doi.org/10.1074/jbc.273.51.34316.

[59] Radhakrishnan A, Ikeda Y, Kwon HJ, Brown MS, Goldstein JL. Sterol-regulated transport of SREBPs from endoplasmic reticulum to Golgi: Oxysterols block transport by binding to Insig. Proc Natl Acad Sci 2007;104:6511–8. https://doi.org/10.1073/pnas.0700899104.

[60] Li Z, Martin M, Zhang J, Huang H-Y, Bai L, Zhang J, Kang J, He M, Li J, Maurya MR, Gupta S, Zhou G, Sangwung P, Xu Y-J, Lei T, Huang H-D, Jain M, Jain MK, Subramaniam S, Shyy JY-J. KLF4 Regulation of Ch25h and LXR Mitigates Atherosclerosis Susceptibility. Circulation 2017;136:1315–30. https://doi.org/10.1161/CIRCULATIONAHA.117.027462.

[61] Lappano R, Recchia AG, De Francesco EM, Angelone T, Cerra MC, Picard D, Maggiolini M. The Cholesterol Metabolite 25-Hydroxycholesterol Activates Estrogen Receptor α-Mediated Signaling in Cancer Cells and in Cardiomyocytes. PLoS ONE 2011;6:e16631. https://doi.org/10.1371/journal.pone.0016631.

[62] Hannedouche S, Zhang J, Yi T, Shen W, Nguyen D, Pereira JP, Guerini D, Baumgarten BU, Roggo S, Wen B, Knochenmuss R, Noël S, Gessier F, Kelly LM, Vanek M, Laurent S, Preuss I, Miault C, Christen I, Karuna R, Li W, Koo D-I, Suply T, Schmedt C, Peters EC, Falchetto R, Katopodis A, Spanka C, Roy M-O, Detheux M, Chen YA, Schultz PG, Cho CY, Seuwen K, Cyster JG, Sailer AW. Oxysterols direct immune cell migration through EBI2. Nature 2011;475:524–7. https://doi.org/10.1038/nature10280.

[63] Liu C, Yang XV, Wu J, Kuei C, Mani NS, Zhang L, Yu J, Sutton SW, Qin N, Banie H, Karlsson L, Sun S, Lovenberg TW. Oxysterols direct B-cell migration through EBI2. Nature 2011;475:519–23. https://doi.org/10.1038/nature10226.

[64] Pokharel SM, Shil NK, Gc JB, Colburn ZT, Tsai S-Y, Segovia JA, Chang T-H, Bandyopadhyay S, Natesan S, Jones JCR, Bose S. Integrin activation by the lipid molecule 25-hydroxycholesterol induces a proinflammatory response. Nat Commun 2019;10:1482. https://doi.org/10.1038/s41467-019-09453-x.

[65] Diczfalusy U, Olofsson KE, Carlsson A-M, Gong M, Golenbock DT, Rooyackers O, Fläring U, Björkbacka H. Marked upregulation of cholesterol 25-hydroxylase expression by lipopolysaccharide. J Lipid Res 2009;50:2258–64. https://doi.org/10.1194/jlr.M900107-JLR200.

[66] Park K, Scott AL. Cholesterol 25-hydroxylase production by dendritic cells and macrophages is regulated by type I interferons. J Leukoc Biol 2010;88:1081–7. https://doi.org/10.1189/jlb.0610318.

[67] Liu Y, Wei Z, Ma X, Yang X, Chen Y, Sun L, Ma C, Miao QR, Hajjar DP, Han J, Duan Y. 25-Hydroxycholesterol activates the expression of cholesterol 25-hydroxylase in an LXR-dependent mechanism. J Lipid Res 2018;59:439–51. https://doi.org/10.1194/jlr.M080440.

[68] Bauman DR, Bitmansour AD, McDonald JG, Thompson BM, Liang G, Russell DW. 25-Hydroxycholesterol secreted by macrophages in response to Toll-like receptor activation suppresses immunoglobulin A production. Proc Natl Acad Sci U S A 2009;106:16764–9. https://doi.org/10.1073/pnas.0909142106.

[69] Rydberg EK, Salomonsson L, Hultén LM, Norén K, Bondjers G, Wiklund O, Björnheden T, Ohlsson BG. Hypoxia increases 25-hydroxycholesterol-induced interleukin-8 protein secretion in human macrophages. Atherosclerosis

2003;170:245–52. https://doi.org/10.1016/S0021-9150(03)00302-2.

[70] Liu Y, Hultén LM, Wiklund O. Macrophages Isolated From Human Atherosclerotic Plaques Produce IL-8, and Oxysterols May Have a Regulatory Function for IL-8 Production. Arterioscler Thromb Vasc Biol 1997;17:317–23. https://doi.org/10.1161/01.ATV.17.2.317.

[71] Liu S-Y, Aliyari R, Chikere K, Li G, Marsden MD, Smith JK, Pernet O, Guo H, Nusbaum R, Zack JA, Freiberg AN, Su L, Lee B, Cheng G. Interferon-Inducible Cholesterol-25-Hydroxylase Broadly Inhibits Viral Entry by Production of 25-Hydroxycholesterol. Immunity 2013;38:92–105. https://doi.org/10.1016/j.immuni.2012.11.005.

[72] Li C, Deng Y-Q, Wang S, Ma F, Aliyari R, Huang X-Y, Zhang N-N, Watanabe M, Dong H-L, Liu P, Li X-F, Ye Q, Tian M, Hong S, Fan J, Zhao H, Li L, Vishlaghi N, Buth JE, Au C, Liu Y, Lu N, Du P, Qin FX-F, Zhang B, Gong D, Dai X, Sun R, Novitch BG, Xu Z, Qin C-F, Cheng G. 25-Hydroxycholesterol Protects Host against Zika Virus Infection and Its Associated Microcephaly in a Mouse Model. Immunity 2017;46:446–56. https://doi.org/10.1016/j.immuni.2017.02.012.

[73] Wang S, Li W, Hui H, Tiwari SK, Zhang Q, Croker BA, Rawlings S, Smith D, Carlin AF, Rana TM. Cholesterol 25-Hydroxylase inhibits SARS-CoV-2 and other coronaviruses by depleting membrane cholesterol. EMBO J 2020;39:e106057. https://doi.org/10.15252/embj.2020106057.

[74] Blanc M, Hsieh WY, Robertson KA, Kropp KA, Forster T, Shui G, Lacaze P, Watterson S, Griffiths SJ, Spann NJ, Meljon A, Talbot S, Krishnan K, Covey DF, Wenk MR, Craigon M, Ruzsics Z, Haas J, Angulo A, Griffiths WJ, Glass CK, Wang Y, Ghazal P. The Transcription Factor STAT-1 Couples Macrophage Synthesis of 25-Hydroxycholesterol to the Interferon Antiviral Response. Immunity 2013;38:106–18. https://doi.org/10.1016/j.immuni.2012.11.004.

[75] Pokharel SM, Chiok K, Shil NK, Mohanty I, Bose S. Tumor Necrosis Factor-alpha utilizes MAPK/NFκB pathways to induce cholesterol-25 hydroxylase for amplifying pro-inflammatory response via 25-hydroxycholesterol-integrin-FAK pathway. PLoS ONE 2021;16:e0257576. https://doi.org/10.1371/journal.pone.0257576.

[76] Poli G, Sottero B, Gargiulo S, Leonarduzzi G. Cholesterol oxidation products in

the vascular remodeling due to atherosclerosis. Mol Aspects Med 2009;30:180–9. https://doi.org/10.1016/j.mam.2009.02.003.

[77] Gargiulo S, Gamba P, Testa G, Leonarduzzi G, Poli G. The role of oxysterols in vascular ageing. J Physiol 2016;594:2095–113. https://doi.org/10.1113/JP271168.

[78] Hodis HN, Crawford DW, Sevanian A. Cholesterol feeding increases plasma and aortic tissue cholesterol oxide levels in parallel: further evidence for the role of cholesterol oxidation in atherosclerosis. Atherosclerosis 1991;89:117–26. https://doi.org/10.1016/0021-9150(91)90051-4.

[79] Canfrán-Duque A, Rotllan N, Zhang X, Andrés-Blasco I, Thompson BM, Sun J, Price NL, Fernández-Fuertes M, Fowler JW, Gómez-Coronado D, Sessa WC, Giannarelli C, Schneider RJ, Tellides G, McDonald JG, Fernández-Hernando C, Suárez Y. Macrophage-Derived 25-Hydroxycholesterol Promotes Vascular Inflammation, Atherogenesis, and Lesion Remodeling. Circulation 2023;147:388–408. https://doi.org/10.1161/CIRCULATIONAHA.122.059062.

[80] Naito Y, Shimozawa M, Kuroda M, Nakabe N, Manabe H, Katada K, Kokura S, Ichikawa H, Yoshida N, Noguchi N, Yoshikawa T. Tocotrienols reduce 25-hydroxycholesterol-induced monocyte–endothelial cell interaction by inhibiting the surface expression of adhesion molecules. Atherosclerosis 2005;180:19–25. https://doi.org/10.1016/j.atherosclerosis.2004.11.017.

[81] Leonarduzzi G, Gamba P, Sottero B, Kadl A, Robbesyn F, Calogero RA, Biasi F, Chiarpotto E, Leitinger N, Sevanian A, Poli G. Oxysterol-induced up-regulation of MCP-1 expression and synthesis in macrophage cells. Free Radic Biol Med 2005;39:1152–61. https://doi.org/10.1016/j.freeradbiomed.2005.06.024.

[82] Biernacka A, Dobaczewski M, Frangogiannis NG. TGF-β signaling in fibrosis. Growth Factors Chur Switz 2011;29:196–202. https://doi.org/10.3109/08977194.2011.595714.

[83] Leonarduzzi G, Sevanian A, Sottero B, Arkan MC, Biasi F, Chiarpotto E, Başağa H, Poli G. Up-regulation of the fibrogenic cytokine TGF-β1 by oxysterols: a mechanistic link between cholesterol and atherosclerosis. FASEB J 2001;15:1619–21. https://doi.org/10.1096/fj.00-0668fje.

[84] Gargiulo S, Sottero B, Gamba P, Chiarpotto E, Poli G, Leonarduzzi G. Plaque oxysterols induce unbalanced up-regulation of matrix metalloproteinase-9 in

macrophagic cells through redox-sensitive signaling pathways: Implications regarding the vulnerability of atherosclerotic lesions. Free Radic Biol Med 2011;51:844–55. https://doi.org/10.1016/j.freeradbiomed.2011.05.030.

[85] Belo VA, Guimarães DA, Castro MM. Matrix Metalloproteinase 2 as a Potential Mediator of Vascular Smooth Muscle Cell Migration and Chronic Vascular Remodeling in Hypertension. J Vasc Res 2015;52:221–31. https://doi.org/10.1159/000441621.

[86] Liao PL, Cheng YW, Li CH, Wang YT, Kang JJ. 7-Ketocholesterol and cholesterol-5α,6α-epoxide induce smooth muscle cell migration and proliferation through the epidermal growth factor receptor/phosphoinositide 3-kinase/Akt signaling pathways. Toxicol Lett 2010;197:88–96. https://doi.org/10.1016/j.toxlet.2010.05.002.

[87] Cox DC, Comai K, Goldstein AL. Effects of cholesterol and 25-hydroxycholesterol on smooth muscle cell and endothelial cell growth. Lipids 1988;23:85–8. https://doi.org/10.1007/BF02535285.

[88] Nishio E, Watanabe Y. Oxysterols Induced Apoptosis in Cultured Smooth Muscle Cells through CPP32 Protease Activation and bcl-2 Protein Downregulation. Biochem Biophys Res Commun 1996;226:928–34. https://doi.org/10.1006/bbrc.1996.1452.

[89] Ares MP, Pörn-Ares MI, Thyberg J, Juntti-Berggren L, Berggren PO, Diczfalusy U, Kallin B, Björkhem I, Orrenius S, Nilsson J. Ca2+ channel blockers verapamil and nifedipine inhibit apoptosis induced by 25-hydroxycholesterol in human aortic smooth muscle cells. J Lipid Res 1997;38:2049–61.

[90] Appukuttan A, Kasseckert SA, Kumar S, Reusch HP, Ladilov Y. Oxysterol-induced apoptosis of smooth muscle cells is under the control of a soluble adenylyl cyclase. Cardiovasc Res 2013;99:734–42. https://doi.org/10.1093/cvr/cvt137.

[91] Perales S, Alejandre MJ, Palomino-Morales R, Torres C, Iglesias J, Linares A. Effect of Oxysterol-Induced Apoptosis of Vascular Smooth Muscle Cells on Experimental Hypercholesterolemia. J Biomed Biotechnol 2009;2009:456208. https://doi.org/10.1155/2009/456208.

[92] Yin J, Chaufour X, McLachlan C, McGuire M, White G, King N, Hambly B. Apoptosis of vascular smooth muscle cells induced by cholesterol and its oxides in

vitro and in vivo. Atherosclerosis 2000;148:365–74. https://doi.org/10.1016/S0021-9150(99)00286-5.

[93] Watson KE, Boström K, Ravindranath R, Lam T, Norton B, Demer LL. TGF-beta 1 and 25-hydroxycholesterol stimulate osteoblast-like vascular cells to calcify. J Clin Invest 1994;93:2106–13. https://doi.org/10.1172/JCI117205.

[94] Liu H, Yuan L, Xu S, Zhang T, Wang K. Cholestane-3beta, 5alpha, 6beta-triol promotes vascular smooth muscle cells calcification. Life Sci 2004;76:533–43. https://doi.org/10.1016/j.lfs.2004.06.025.

[95] Saito E, Wachi H, Sato F, Seyama Y. 7-ketocholesterol, a major oxysterol, promotes pi-induced vascular calcification in cultured smooth muscle cells. J Atheroscler Thromb 2008;15:130–7. https://doi.org/10.5551/jat.e556.

[96] Dong Q, Chen Y, Liu W, Liu X, Chen A, Yang X, Li Y, Wang S, Fu M, Ou J-S, Lu L, Yan J. 25-Hydroxycholesterol promotes vascular calcification via activation of endoplasmic reticulum stress. Eur J Pharmacol 2020;880:173165. https://doi.org/10.1016/j.ejphar.2020.173165.

[97] Krut LH. Clearance of subcutaneous implants of cholesterol in the rat promoted by oxidation products of cholesterol. A postulated role for oxysterols in preventing atherosclerosis. Atherosclerosis 1982;43:105–18. https://doi.org/10.1016/0021-9150(82)90103-4.

[98] Olkkonen VM. Macrophage oxysterols and their binding proteins: roles in atherosclerosis. Curr Opin Lipidol 2012;23:462. https://doi.org/10.1097/MOL.0b013e328356dba0.

[99] Gold ES, Ramsey SA, Sartain MJ, Selinummi J, Podolsky I, Rodriguez DJ, Moritz RL, Aderem A. ATF3 protects against atherosclerosis by suppressing 25-hydroxycholesterol–induced lipid body formation. J Exp Med 2012;209:807–17. https://doi.org/10.1084/jem.20111202.

[100] Liu Z-Y, Liu F, Cao Y, Peng S-L, Pan H-W, Hong X-Q, Zheng P-F. ACSL1, CH25H, GPCPD1, and PLA2G12A as the potential lipid-related diagnostic biomarkers of acute myocardial infarction. Aging 2023;15:1394–411. https://doi.org/10.18632/aging.204542.

[101] Shen C, Zhou J, Wang X, Yu X-Y, Liang C, Liu B, Pan X, Zhao Q, Song JL, Wang J, Bao M, Wu C, Li Y, Song Y-H. Angiotensin-II-induced Muscle Wasting is

Mediated by 25-Hydroxycholesterol via GSK3β Signaling Pathway. EBioMedicine 2017;16:238–50. https://doi.org/10.1016/j.ebiom.2017.01.040.

[102] Elliott KJ, Eguchi S. In Vitro Assays to Determine Smooth Muscle Cell Hypertrophy, Protein Content, and Fibrosis. Methods Mol Biol Clifton NJ 2017;1614:147–53. https://doi.org/10.1007/978-1-4939-7030-8_11.

[103] Kovács KB, Szalai L, Szabó P, Gém JB, Barsi S, Szalai B, Perey-Simon B, Turu G, Tóth AD, Várnai P, Hunyady L, Balla A. An Unexpected Enzyme in Vascular Smooth Muscle Cells: Angiotensin II Upregulates Cholesterol-25-Hydroxylase Gene Expression. Int J Mol Sci 2023;24:3968. https://doi.org/10.3390/ijms24043968.

[104] Schindelin J, Arganda-Carreras I, Frise E, Kaynig V, Longair M, Pietzsch T, Preibisch S, Rueden C, Saalfeld S, Schmid B, Tinevez J-Y, White DJ, Hartenstein V, Eliceiri K, Tomancak P, Cardona A. Fiji: an open-source platform for biological-image analysis. Nat Methods 2012;9:676–82. https://doi.org/10.1038/nmeth.2019.

[105] Bolte S, Cordelières F. A guided tour into subcellular colocalization analysis in light microscopy. J Microsc 2006;224:213–32. https://doi.org/10.1111/j.1365-2818.2006.01706.x.

[106] Poli G, Biasi F, Leonarduzzi G. Oxysterols in the pathogenesis of major chronic diseases. Redox Biol 2013;1:125–30. https://doi.org/10.1016/j.redox.2012.12.001.

[107] Bakris G, Gradman A, Reif M, Wofford M, Munger M, Harris S, Vendetti J, Michelson EL, Wang R. Antihypertensive Efficacy of Candesartan in Comparison to Losartan: The CLAIM Study. J Clin Hypertens 2001;3:16–21. https://doi.org/10.1111/j.1524-6175.2001.00826.x.

[108] Violin JD, DeWire SM, Yamashita D, Rominger DH, Nguyen L, Schiller K, Whalen EJ, Gowen M, Lark MW. Selectively engaging beta-arrestins at the angiotensin II type 1 receptor reduces blood pressure and increases cardiac performance. J Pharmacol Exp Ther 2010;335:572–9. https://doi.org/10.1124/jpet.110.173005.

[109] Devost D, Sleno R, Pétrin D, Zhang A, Shinjo Y, Okde R, Aoki J, Inoue A, Hébert TE. Conformational Profiling of the AT1 Angiotensin II Receptor Reflects Biased Agonism, G Protein Coupling, and Cellular Context. J Biol Chem 2017;292:5443–

56. https://doi.org/10.1074/jbc.M116.763854.

[110] Szakadáti G, Tóth AD, Oláh I, Erdélyi LS, Balla T, Várnai P, Hunyady L, Balla A. Investigation of the Fate of Type I Angiotensin Receptor after Biased Activation. Mol Pharmacol 2015;87:972–81. https://doi.org/10.1124/mol.114.097030.

[111] Turu G, Balla A, Hunyady L. The Role of β-Arrestin Proteins in Organization of Signaling and Regulation of the AT1 Angiotensin Receptor. Front Endocrinol 2019;10:519. https://doi.org/10.3389/fendo.2019.00519.

[112] Yamauchi J, Nagao M, Kaziro Y, Itoh H. Activation of p38 Mitogen-activated Protein Kinase by Signaling through G Protein-coupled Receptors: INVOLVEMENT OF Gβγ AND Gαq/11 SUBUNITS *. J Biol Chem 1997;272:27771–7. https://doi.org/10.1074/jbc.272.44.27771.

[113] Nagao M, Yamauchi J, Kaziro Y, Itoh H. Involvement of Protein Kinase C and Src Family Tyrosine Kinase in Gαq/11-induced Activation of c-Jun N-terminal Kinase and p38 Mitogen-activated Protein Kinase. J Biol Chem 1998;273:22892–8. https://doi.org/10.1074/jbc.273.36.22892.

[114] Caunt CJ, Keyse SM. Dual-specificity MAP kinase phosphatases (MKPs): shaping the outcome of MAP kinase signalling. FEBS J 2013;280:489–504. https://doi.org/10.1111/j.1742-4658.2012.08716.x.

[115] Amit I, Citri A, Shay T, Lu Y, Katz M, Zhang F, Tarcic G, Siwak D, Lahad J, Jacob-Hirsch J, Amariglio N, Vaisman N, Segal E, Rechavi G, Alon U, Mills GB, Domany E, Yarden Y. A module of negative feedback regulators defines growth factor signaling. Nat Genet 2007;39:503–12. https://doi.org/10.1038/ng1987.

[116] Komati R, Spadoni D, Zheng S, Sridhar J, Riley KE, Wang G. Ligands of Therapeutic Utility for the Liver X Receptors. Mol J Synth Chem Nat Prod Chem 2017;22:88. https://doi.org/10.3390/molecules22010088.

[117] Augsburger F, Filippova A, Rasti D, Seredenina T, Lam M, Maghzal G, Mahiout Z, Jansen-Dürr P, Knaus UG, Doroshow J, Stocker R, Krause K-H, Jaquet V. Pharmacological characterization of the seven human NOX isoforms and their inhibitors. Redox Biol 2019;26:101272. https://doi.org/10.1016/j.redox.2019.101272.

[118] Reis J, Massari M, Marchese S, Ceccon M, Aalbers FS, Corana F, Valente S, Mai A, Magnani F, Mattevi A. A closer look into NADPH oxidase inhibitors:

Validation and insight into their mechanism of action. Redox Biol 2020;32:101466. https://doi.org/10.1016/j.redox.2020.101466.

[119] Wu N, Ye C, Zheng F, Wan G-W, Wu L-L, Chen Q, Li Y-H, Kang Y-M, Zhu G-Q. MiR155-5p Inhibits Cell Migration and Oxidative Stress in Vascular Smooth Muscle Cells of Spontaneously Hypertensive Rats. Antioxidants 2020;9:204. https://doi.org/10.3390/antiox9030204.

[120] Madenspacher JH, Morrell ED, Gowdy KM, McDonald JG, Thompson BM, Muse G, Martinez J, Thomas S, Mikacenic C, Nick JA, Abraham E, Garantziotis S, Stapleton RD, Meacham JM, Thomassen MJ, Janssen WJ, Cook DN, Wurfel MM, Fessler MB. Cholesterol 25-hydroxylase promotes efferocytosis and resolution of lung inflammation. JCI Insight 2020;5:e137189. https://doi.org/10.1172/jci.insight.137189.

[121] Li X, Zhang L, Shi X, Liao T, Zhang N, Gao Y, Xing R, Wang P. MicroRNA-10a-3p Improves Cartilage Degeneration by Regulating CH25H-CYP7B1-RORα Mediated Cholesterol Metabolism in Knee Osteoarthritis Rats. Front Pharmacol 2021;12:690181. https://doi.org/10.3389/fphar.2021.690181.

[122] Zhang Y, Cho Y-Y, Petersen BL, Zhu F, Dong Z. Evidence of STAT1 phosphorylation modulated by MAPKs, MEK1 and MSK1. Carcinogenesis 2004;25:1165–75. https://doi.org/10.1093/carcin/bgh115.

[123] Izumi Y, Cashikar A, Krishnan K, Paul SM, Covey DF, Mennerick SJ, Zorumski CF. A Pro-inflammatory Stimulus Disrupts Hippocampal Plasticity and Learning via Microglial Activation and 25-Hydroxycholesterol. J Neurosci 2021. https://doi.org/10.1523/JNEUROSCI.1502-21.2021.

[124] Pickering JG, Chow LH, Li S, Rogers KA, Rocnik EF, Zhong R, Chan BMC. α5β1 Integrin Expression and Luminal Edge Fibronectin Matrix Assembly by Smooth Muscle Cells after Arterial Injury. Am J Pathol 2000;156:453–65. https://doi.org/10.1016/S0002-9440(10)64750-5.

[125] Song Y, Qin X, Wang H, Miao R, Zhang Y, Miao C, Wang Z. Effects of integrin α5β1 on the proliferation and migration of human aortic vascular smooth muscle cells. Mol Med Rep 2016;13:1147–55. https://doi.org/10.3892/mmr.2015.4649.

9. Bibliography of the candidate's publications

9.1. Publications relevant to the dissertation

I. **Kovács, Kinga Bernadett** ; Szalai, Laura ; Szabó, Pál ; Gém, Janka Borbála ; Barsi, Szilvia ; Szalai, Bence ; Perey-Simon, Bernadett ; Turu, Gábor ; Tóth, András Dávid ; Várnai, Péter ; Hunyady, László ; Balla, András. An Unexpected Enzyme in Vascular Smooth Muscle Cells: Angiotensin II Upregulates Cholesterol-25-Hydroxylase Gene Expression
International Journal of Molecular Sciences, 2023, 24.4: 3968. **IF(2023): 4.9**

II. Gém, Janka Borbála ; **Kovács, Kinga Bernadett*** ; Szalai, Laura ; Szakadáti, Gyöngyi ; Porkoláb, Edit ; Szalai, Bence ; Turu, Gábor ; Tóth, András Dávid ; Szekeres, Mária ; Hunyady, László ; Balla, András. Characterization of Type 1 Angiotensin II Receptor Activation Induced Dual-Specificity MAPK Phosphatase Gene Expression Changes in Rat Vascular Smooth Muscle Cells
Cells, 2021, 10.12: 3538. **IF(2021): 7.666**

Cumulative impact factor: 12.566

9.2. Publications unrelated to the dissertation

I. Szalai, Laura ; Sziráki, András* ; Erdélyi, László Sándor ; **Kovács, Kinga Bernadett** ; Tóth, Miklós ; Tóth, András Dávid ; Turu, Gábor ; Bonnet, Dominique ; Mouillac, Bernard ; Hunyady, László ; Balla, András. Functional Rescue of a Nephrogenic Diabetes Insipidus Causing Mutation in the V2 Vasopressin Receptor by Specific Antagonist and Agonist Pharmacochaperones
Frontiers in Pharmacology, 2022, 13: 811836. **IF(2022): 5,6**

II. Bugyi, Fanni ; Tóth, Gábor ; **Kovács, Kinga Bernadett** ; Drahos, László ; Turiák, Lilla. Comparison of solid-phase extraction methods for efficient purification of phosphopeptides with low sample amounts
Journal of Chromatography A, 2022, 1685: 463597. **IF(2022): 4.1**

III. Vass, Zsolt ; Shenker-Horváth, Kinga ; Bányai, Bálint ; Vető, Kinga Nóra ; Török, Viktória ; Gém, Janka Borbála ; Nádasy, György L. ; **Kovács, Kinga Bernadett** ; Horváth, Eszter Mária ; Jakus, Zoltán ; Hunyady, László ; Szekeres, Mária ; Dörnyei, Gabriella. Investigating the Role of Cannabinoid Type 1 Receptors in

Vascular Function and Remodeling in a Hypercholesterolemic Mouse Model with Low-Density Lipoprotein–Cannabinoid Type 1 Receptor Double Knockout Animals

International Journal of Molecular Sciences, 2024, 25.17:9537. **IF(2023): 4.9**

Cumulative impact factor of all publications: 27.166

Cumulative impact factor of first author and shared first author publications: 12.566

10. Acknowledgements

First and foremost, I am indebted to my supervisor, András Balla, who has been guiding me in the world of science throughout my TDK and PhD years and helped me with his insightful advice during my research work. I am grateful to Prof. László Hunyady and Prof. Attila Mócsai, who enabled my work in the Department of Physiology and gave me an opportunity to be trained here.

I am thankful for all the practical knowledge and support I received from Laura Szalai, Eszter Halász, and Ilona Oláh, which was fundamental at the beginning of my training in the laboratory and has been extremely useful and cherished ever since. I appreciate the valuable help of Szilvia Barsi and Bence Szalai and the fact that they have always been eager to help when I sought their advice. I am most grateful to all my colleagues and co-authors at the Department and outside of it, who accompanied and helped me along the way.

Lastly, I am beholden to my family and friends for their encouragement, support and trust throughout my studies. I am especially thankful to my fiancé, Tamás Lévai, for his caring support, for his constructive criticisms and appreciation of my scientific work.